Short Communication

Tutorial on Fourier and Hankel Transforms for Ultrafast Optics

Yi-Hao Chen[1]

1. School of Applied and Engineering Physics, Cornell University, United States

This tutorial is designed for individuals who are new to the field of ultrafast optics. It was written in response to the apparent lack of comprehensive introductions to the basic Fourier transform, extending beyond the flat-phase description. Additionally, there is a need for complete derivations of several relations involving the Fourier transform, maintaining its most general formulation. This approach avoids the arbitrary selection of Fourier-transform constants and ensures a complete understanding. It shows the importance of having Fourier-transform constants as parameters. Most important of all, there have been misuse of Fourier transform from my observations, which cannot be easily detected by checking the smoothness of the result of a numerical implementation or by seeing if the simulation duplicates the "overall physics." This problem should be easily solved by a simple tutorial (see Sec. 2.2). I hope that this tutorial can help people understand more about the Fourier transform, especially in the context of ultrafast optics. In addition, a tutorial of the Hankel transform, which arises from the two-dimensional spatial Fourier transform of a radially-symmetric function, is provided. Its numerical implementation based on the fast Hankel transform with high accuracy is also provided, which is the core element of fast radially-symmetric full-field ultrafast propagation.
Feel me to send me an email if there is any confusion, or you think that there is more to add to this tutorial. For a deeper understanding into the ultrafast pulse propagation that involves these transforms, please check out our publicly-shared Github code.

Corresponding author: Yi-Hao Chen, yc2368@cornell.edu

1. Analytic signal

A. Introduction

When we learn ultrafast optics with textbooks, such as Boyd's Nonlinear Optics[1], they usually start with the field equation for the real-valued field:

$$\begin{aligned}\mathrm{E}(t) &= \frac{1}{2}(\mathcal{E}(t)+\mathcal{E}^*(t)) = \frac{1}{2}\left(E(t)e^{-i\omega_0 t}+E^*(t)e^{i\omega_0 t}\right)\\ &= \mathrm{Re}\left[\mathcal{E}(t)\right] \qquad \text{(S1)}\end{aligned}$$

or simply assume, for the complex-valued field:

$$\mathcal{E}(t) = E(t)e^{-i\omega_0 t}. \qquad \text{(S2)}$$

 doi.org/10.32388/JFPRSL.2

These two equations make intuitive sense if the field is a simple sinusoidal wave that follows $\mathrm{E}(t) = \sin(\omega_0 t) = \frac{e^{i\omega_0 t} - e^{-i\omega_0 t}}{2i}$ so that the coefficient $E(t)$ in Eq. (S1) is just $\frac{-1}{2i}$. However, in general situations of real-valued $\mathrm{E}(t)$, there are infinite possible options for complex-valued $\mathcal{E}(t)$ that satisfies Eq. (S1). During nonlinear studies, there are usually conversions between temporal and spectral components through the Fourier transform. Not correctly defining or understanding the decomposition of the field following the form of Eq. (S1) can not only result in a mixed use of Fourier transform of the real-valued $\mathrm{E}(t)$ and complex-valued $\mathcal{E}(t)$ (which will be discussed in detail in Fig. S1) but also mislead researchers from obtaining all generated frequencies, leading to the problem with missing negative frequencies[2]. Therefore, it is important to understand and apply the correct decomposition. Here I will introduce the "analytic-signal decomposition," which decomposes the real-valued signal into its positive- and negative-frequency components. The positive-frequency part is called the "analytic signal," whose complex conjugate is the negative-frequency part of the real-valued signal.

An analytic signal is a complex-valued function that has no negative-frequency part. If $s(t)$ is a real-valued function with Fourier transform $\mathfrak{F}[s] = S(f)$, then it exhibits the Hermitian symmetry about $\nu = 0$.

$$S(-\nu) = S^*(\nu). \tag{S3}$$

Thus, there is redundancy if both frequencies are considered; negative-frequency components can be discarded without loss of information.

We define $S_a(\nu)$ to represent the positive-frequency part as the following:

$$\begin{aligned} S_a(\nu) &= \begin{cases} 2S(\nu), & \nu > 0 \\ S(\nu), & \nu = 0 \\ 0, & \nu < 0 \end{cases} \\ &= S(\nu) + \mathrm{sgn}(\nu) S(\nu), \end{aligned} \tag{S4}$$

so that

$$\begin{aligned} S(\nu) &= \begin{cases} \frac{1}{2} S_a(\nu), & \nu > 0 \\ S_a(\nu), & \nu = 0 \\ \frac{1}{2} S_a^*(-\nu), & \nu < 0 \end{cases} \\ &= \frac{1}{2}\left(S_a(\nu) + S_a^*(-\nu)\right) \end{aligned} \tag{S5}$$

and thus

$$s(t) = \frac{1}{2}\left(s_a(t) + s_a^*(t)\right). \tag{S6}$$

$s(t)$ is a combination of its analytic signal $s_a(t)$ and the corresponding complex conjugate, which is the negative-frequency part of the $s(t)$.

Since analytic signal of $s(t)$ is the inverse Fourier transform of $S_a(\nu)$,

$$\begin{aligned} s_a(t) &= \mathfrak{F}^{-1}[S(\nu) + \mathrm{sgn}(\nu) S(\nu)] \\ &= s(t) + \mathfrak{F}^{-1}[C_{\mathfrak{F}} \mathfrak{F}^{-1}[\mathrm{sgn}(\nu)] * \mathfrak{F}^{-1}[S(\nu)]] \quad \text{with the convolution theorem [Eq. (S10a)]} \\ &= s(t) + C_{\mathfrak{F}}[C_{\mathfrak{I}\mathfrak{F}} c_s \frac{2}{it} * s(t)] \quad \because \mathfrak{F}^{-1}[f] = C_{\mathfrak{I}\mathfrak{F}} c_s \frac{2}{it} \\ &= s(t) + [-\frac{i c_s}{\pi t} * s(t)], \quad \because C_{\mathfrak{F}} C_{\mathfrak{I}\mathfrak{F}} = \frac{1}{2\pi} \end{aligned} \tag{S7}$$

Any real-valued signal can be decomposed into its positive-frequency (analytic-signal) and negative-frequency parts, which underlies the decomposition of Eq. (S1). In addition, this tells us that the Fourier transform of the real-valued field $\mathbb{E}(t)$ is different from that of the analytic signal $\mathcal{E}(t)$; they exhibit different spectral components. Hence, it is crucial to define clearly what is being used, especially in studies of, for example, four-wave mixing and Raman scattering that involves nonlinear evolutions of different frequencies. In principle, any derivations of nonlinear optics should start with the real-valued signal, followed by its decomposition into the "analytic signal." If a derivation starts directly with a single complex-valued signal (either the positive- or negative-frequency part), then readers need to be cautious about two things: (1) whether there is any missing frequency component due to ignoring the complex-conjugate part, and (2) whether there is a deviation of a factor of 2. As an example, [3] starts with the complex-valued field for deriving the Raman-induced index change, which eventually results in a reported deviation of a factor of 2 between their theory and experiments. (Correct derivation with analytic signal, as well as generalization to an arbitrary polarization, is in [4].) As another example, the third-order nonlinear polarization $\vec{\mathbb{P}}(t)=\int_{-\infty}^{\infty}\chi^{(3)}(t_1,t_2,t_3)\vdots\vec{\mathbb{E}}(t-t_1)\vec{\mathbb{E}}(t-t_2)\vec{\mathbb{E}}(t-t_3)dt_1dt_2dt_3$ is apparently different from $\vec{\mathcal{P}}'(t)=\int_{-\infty}^{\infty}\chi^{(3)}(t_1,t_2,t_3)\vdots\vec{\mathcal{E}}(t-t_1)\vec{\mathcal{E}}(t-t_2)\vec{\mathcal{E}}(t-t_3)dt_1dt_2dt_3$, as $\vec{\mathcal{P}}'(t)$ lacks all frequency components that result from combinations including the negative-frequency components of three $\vec{\mathbb{E}}(t)$'s. Therefore, $\vec{\mathcal{P}}'(t)$ is not the correct calculation for the analytic signal $\vec{\mathcal{P}}(t)$ of $\vec{\mathbb{P}}(t)$. A correct $\vec{\mathcal{P}}(t)$ should be calculated by identifying the positive-frequency part of $\vec{\mathbb{P}}(t)=\frac{1}{2}\left(\vec{\mathcal{P}}(t)+\vec{\mathcal{P}}^*(t)\right)=\int_{-\infty}^{\infty}\chi^{(3)}(t_1,t_2,t_3)\vdots\vec{\mathbb{E}}(t-t_1)\vec{\mathbb{E}}(t-t_2)\vec{\mathbb{E}}(t-t_3)dt_1dt_2dt_3$.

B. Offset frequency $\Omega=\omega-\omega_0$

Applying analytic signal provides benefits in numerical computations. Because real-valued signal contains both positive and negative frequencies, its frequency window should cover both signs of frequency [Fig. S1(a)]. By extracting ω_0 out as in Eq. (S1), the Fourier transform of $E(t)$ (to obtain $E(\Omega)=\mathfrak{F}[E]=C_{\mathfrak{F}}\int_{-\infty}^{\infty}E(t)e^{ic_s\Omega t}dt$ [Eq. (S8)]) is equivalent to applying it with respect to the offset frequency $\Omega=\omega-\omega_0$ [Fig. S1(b)]. The offset center of the frequency window, from $\omega=0$ to ω_0, enables a small window covering only around the signal's spectrum, free from the redundant negative-frequency components. As an example, a broadband simulation of a Yb-doped fiber laser requires a 100-THz window to cover signals from 1--1.2 μm without inducing aliasing.[1] On the other hand, the frequency window of the real-valued $\mathbb{E}(t)$ should be $\sim$ 700-THz wide for a 1-μm ($\approx$ 300 THz) pulse (if we assume the same 100-THz coverage around the signal: $700=2\times300+100$). If ω_0 is the pulse's center frequency, $E(t)$ is called the "slowly-varying" envelope of $\mathcal{E}(t)$. $E(t)$ can be real-valued if the analytic signal $\mathcal{E}(t)$ exhibits no extra phase variation other than sinusoidal waves. Thus, the frequency window of the analytic signal's envelope is 7 times smaller than that of the real-valued signal, allowing a numerical simulation with a larger temporal sampling period and thus less sampling points. For narrowband simulations, the computational improvement can be more significant (an improvement factor of $\frac{600+x}{x}$ with a small x, the size of the narrowband-signal's frequency window). In general, ω_0 does not need to be at the pulse's center frequency. For broadband nonlinear processes such as vibrational-Raman generation in H_2 that creates frequency 125 THz apart from the pump frequency[5][6], or $\geq$ 250 THz for cascaded processes[7][8], ω_0 should be placed such that the frequency window can cover all generated frequency components.

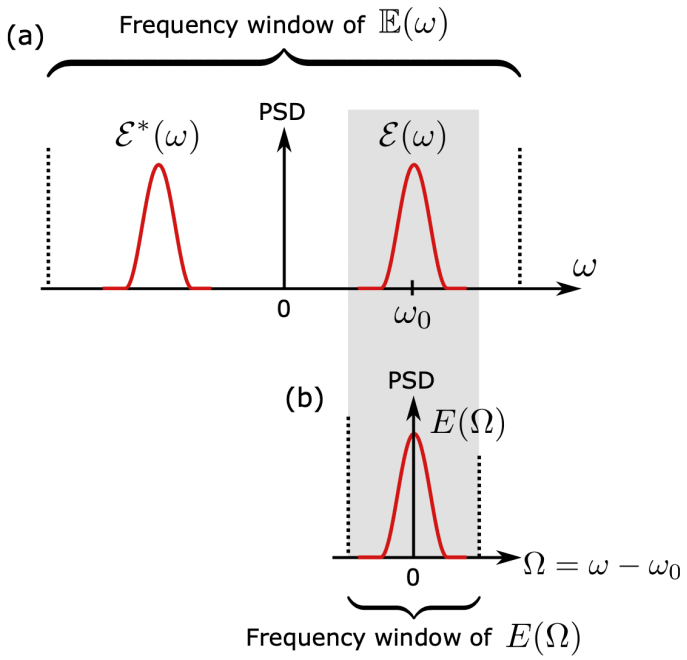

Figure S1. Spectral domain of the Fourier-transform components of (a) the real-valued signal and (b) the envelope of its analytic signal [Eq. (S1)]. PSD: power spectral density $\sim |\mathfrak{F}[\cdot]|^2$

2. Spectral Fourier transform

In this section, we explain the Fourier transform in its continuous and discrete formats. In addition, all constants are represented as parameters to be compatible with various conventions people in different fields use. I would also like to advocate people to derive their equations based on parametrized Fourier transform, as in Eq. (S8). As I will show later, many relations are dependent on the Fourier-transform convention and its constants. Various conventions out there in the world (e.g., $C_{\mathfrak{F}} = 1$ or $C_{\mathfrak{F}} = \frac{1}{\sqrt{2\pi}}$ [Eq. (S8)]) can create misleading equations. For example, if an equation has π, we do not know whether it is dependent on Fourier-transform constants or not; it can come from anywhere, such as the frequency relation $\omega = 2\pi\nu$ that is irrelevant to Fourier transform. Furthermore, losing the information of Fourier-transform constants prevents people from correctly transforming the equation from continuous to discrete Fourier transform for numerical computations, as I would show later in Sec. 2.2.

Here in this tutorial, the overall trend of notation follows the physical convention whose inverse spectral Fourier transform follows $A(t) \sim \int A(\omega) e^{i(k_z z - \omega t)} d\omega$, which is the spectral Fourier transform in mathematics or engineering. Note that in contrast to the spectral Fourier transform, the physical convention ($k_z z - \omega t$) potentially shows that the spatial Fourier transform $\mathfrak{F}_{k_z}$ is consistent with mathematical convention; however, we typically do not calculate based on the k_z-space. Here, we will focus only on spectral Fourier transform.

doi.org/10.32388/JFPRSL.2

2.1. Definition

In general, the Fourier transform is defined as

$$\begin{aligned} A(\omega) &= \mathfrak{F}[A(t)] \equiv C_{\mathfrak{F}} \int_{-\infty}^{\infty} A(t) e^{ic_s \omega t} dt \\ A(t) &= \mathfrak{F}^{-1}[A(\omega)] \equiv C_{\mathfrak{IF}} \int_{-\infty}^{\infty} A(\omega) e^{-ic_s \omega t} d\omega. \end{aligned} \tag{S8}$$

If $c_s = 1$, the Fourier transform follows the physical convention; whereas it follows the mathematical convention if it is -1. Its constants satisfy $C_{\mathfrak{F}} C_{\mathfrak{IF}} = \frac{1}{2\pi}$, which is found with

$$\begin{aligned} A(t) &= C_{\mathfrak{IF}} \int_{-\infty}^{\infty} A(\omega) e^{-ic_s \omega t} d\omega \\ &= C_{\mathfrak{IF}} \int_{-\infty}^{\infty} \left(C_{\mathfrak{F}} \int_{-\infty}^{\infty} A(\tau) e^{ic_s \omega \tau} d\tau \right) e^{-ic_s \omega t} d\omega \\ &= C_{\mathfrak{F}} C_{\mathfrak{IF}} \int_{-\infty}^{\infty} \int_{-\infty}^{\infty} A(\tau) e^{ic_s \omega (\tau - t)} d\omega d\tau \\ &= C_{\mathfrak{F}} C_{\mathfrak{IF}} \int_{-\infty}^{\infty} A(\tau) \frac{2\pi}{c_s} \delta(\tau - t) d\tau \\ &= C_{\mathfrak{F}} C_{\mathfrak{IF}} A(t) 2\pi \quad \because c_s = 1 \\ \Rightarrow C_{\mathfrak{F}} C_{\mathfrak{IF}} &= \frac{1}{2\pi}. \end{aligned} \tag{S9}$$

Since the convolution theorem is a commonly-used relation, we show it below:

$$\mathfrak{F}[A * B] = \frac{1}{C_{\mathfrak{F}}} \mathfrak{F}[A] \mathfrak{F}[B] \tag{S10a}$$

$$\mathfrak{F}^{-1}[A * B] = \frac{1}{C_{\mathfrak{IF}}} \mathfrak{F}^{-1}[A] \mathfrak{F}^{-1}[B], \tag{S10b}$$

where the convolution (denoted with $*$) follows

$$(A * B)(t) \equiv \int_{-\infty}^{\infty} A(\tau) B(t - \tau) d\tau. \tag{S11}$$

The discrete counterpart is

$$\begin{aligned} \mathfrak{F}_{D_c}[A * B] &= \frac{1}{C_{\mathfrak{F}}} \mathfrak{F}_{D_c}[A] \mathfrak{F}_{D_c}[B] \\ \mathfrak{F}_{D_c}^{-1}[A * B] &= \frac{1}{C_{\mathfrak{IF}}} \mathfrak{F}_{D_c}^{-1}[A] \mathfrak{F}_{D_c}^{-1}[B] \end{aligned} \quad \text{if} \quad \begin{aligned} A(\omega) &= \mathfrak{F}_{D_c}[A(t_n)] \equiv C_{\mathfrak{F}} \sum_{n=1}^{\mathfrak{N}} A(t_n) e^{ic_s \omega t_n} \triangle t \\ A(t) &= \mathfrak{F}_{D_c}^{-1}[A(\omega_m)] \equiv C_{\mathfrak{IF}} \sum_{m=1}^{\mathfrak{N}} A(\omega_m) e^{-ic_s \omega_m t} \triangle \omega \end{aligned} . \tag{S12}$$

$\mathfrak{F}$ and $\mathfrak{F}_{D_c}$ are the continuous and discrete versions of Fourier transform, respectively. $\mathfrak{N}$ is the number of discrete points. In the discrete manner, $t_n = n \triangle t$ and $\omega_m = m \triangle \omega$. The time window is $T^w = \mathfrak{N} \triangle t$, and the frequency window $\nu^w = \frac{1}{\triangle t} = \frac{\mathfrak{N}}{T^w} = \mathfrak{N} \triangle \nu$. The angular-frequency spacing $\triangle w = 2\pi \triangle \nu = \frac{2\pi}{T^w}$. If the sampling frequency is high enough, $\mathfrak{F}_{D_c}[\cdot] \approx \mathfrak{F}[\cdot]$ and $\mathfrak{F}_{D_c}^{-1}[\cdot] \approx \mathfrak{F}^{-1}[\cdot]$.

In practice, during numerical computations, we sloppily treat the result from the following discrete Fourier transform (DFT) simply as Fourier transform:

$$\begin{aligned} A_D(\omega) &= \mathfrak{F}_D[A(t_n)] \equiv C_{\mathfrak{F}_D} \sum_{n=1}^{\mathfrak{N}} A(t_n) e^{ic_s \omega t_n} \\ A(t) &= \mathfrak{F}_D^{-1}[A_D(\omega_m)] \equiv C_{\mathfrak{IF}_D} \sum_{m=1}^{\mathfrak{N}} A_D(\omega_m) e^{-ic_s \omega_m t}, \end{aligned} \tag{S13}$$

which differs from the Fourier transform [Eq. (S12)] in constants and units:

$$\mathfrak{F} = \frac{C_{\mathfrak{F}}}{C_{\mathfrak{F}_D}} \triangle t\mathfrak{F}_D \tag{S14a}$$

$$\mathfrak{F}^{-1} = \frac{C_{\mathfrak{I}\mathfrak{F}}}{C_{\mathfrak{I}\mathfrak{F}_D}} \triangle \omega\mathfrak{F}_D^{-1}. \tag{S14b}$$

If we replace variables following $\omega_m = m \triangle \omega = m\frac{2\pi}{T^w} = m\frac{2\pi}{\mathfrak{N}\triangle t}$ and $t_n = n \triangle t$, Eq. (S13) becomes

$$\begin{aligned} A_D(\omega_m) = \mathfrak{F}_D[A(t_n)] &\equiv C_{\mathfrak{F}_D}\sum_{n=1}^{\mathfrak{N}} A(t_n)e^{ic_s\frac{2\pi}{\mathfrak{N}}mn} \\ A(t_n) = \mathfrak{F}_D^{-1}[A_D(\omega_m)] &\equiv C_{\mathfrak{I}\mathfrak{F}_D}\sum_{m=1}^{\mathfrak{N}} A_D(\omega_m)e^{-ic_s\frac{2\pi}{\mathfrak{N}}nm}, \end{aligned} \tag{S15}$$

where $C_{\mathfrak{F}_D}C_{\mathfrak{I}\mathfrak{F}_D} = \frac{1}{\mathfrak{N}}$, found with the similar process to Eq. (S9).

The DFT $A_D(\omega)$ [Eq. (S13)] is denoted with an extra "D" subscript to distinguish it from $A(\omega)$ of Eqs. (S8) and (S12). Therefore, it is important to derive a relationship between $A(\omega)$ and $A_D(\omega)$, which follows

$$\frac{1}{C_{\mathfrak{F}_D}}A_D(\omega) \triangle t = \frac{1}{C_{\mathfrak{F}}}A(\omega) \tag{S16}$$

so that they obtain the same $A(t)$. For the commonly-used Fourier-transform convention in the laser field (and the one we emphasize in this article), $c_s = 1$ so that the inverse Fourier transform is consistent with the use of $A(t) \sim \int A(\omega)e^{i(k_z z-\omega t)}d\omega$ in physical representation. With this convention, the inverse Fourier transform in mathematics becomes the Fourier transform in physics, so we define $C_{\mathfrak{F}_D} = \frac{1}{\mathfrak{N}}$, the constant of the mathematical inverse DFT, such that Eq. (S16) becomes $A_D(\omega) = A(\omega) \triangle \nu/C_{\mathfrak{F}}$ in this convention.

With Eqs. (S10) and (S14), DFT's convolution theorem follows

$$\mathfrak{F}_D[A * B] = \frac{\Delta t}{C_{\mathfrak{F}_D}}\mathfrak{F}_D[A]\mathfrak{F}_D[B] \tag{S17a}$$

$$\mathfrak{F}_D^{-1}[A * B] = \frac{\Delta \omega}{C_{\mathrm{Im}\mathfrak{F}_D}}\mathfrak{F}_D^{-1}[A]\mathfrak{F}_D^{-1}[B]. \tag{S17b}$$

In addition to convolution [Eq. (S11)], here I introduce "cross correlation" that is less-frequently used. It is denoted with $\star$ and follows

$$(A \star B)(t) \equiv \int_{-\infty}^{\infty} \overline{A(\tau)}B(t+\tau)d\tau. \tag{S18}$$

It satisfies

$$\mathfrak{F}[A \star B] = \frac{1}{C_{\mathfrak{F}}}\overline{\mathfrak{F}[A]}\mathfrak{F}[B] \tag{S19a}$$

$$\mathfrak{F}^{-1}[A \star B] = \frac{1}{C_{\mathrm{Im}\mathfrak{F}}}\overline{\mathfrak{F}^{-1}[A]}\mathfrak{F}^{-1}[B]. \tag{S19b}$$

Similarly, its discrete counterpart is

$$\mathfrak{F}_D[A \star B] = \frac{\Delta t}{C_{\mathfrak{F}_D}}\overline{\mathfrak{F}_D[A]}\mathfrak{F}_D[B] \overset{also}{=} \frac{\Delta t}{C_{\mathrm{Im}\mathfrak{F}_D}}\mathfrak{F}_D^{-1}[\overline{A}]\mathfrak{F}_D[B] \tag{S20a}$$

$$\mathfrak{F}_D^{-1}[A \star B] = \frac{\Delta \omega}{C_{\mathrm{Im}\mathfrak{F}_D}}\overline{\mathfrak{F}_D^{-1}[A]}\mathfrak{F}_D^{-1}[B] \overset{also}{=} \frac{\Delta \omega}{C_{\mathfrak{F}_D}}\mathfrak{F}_D[\overline{A}]\mathfrak{F}_D^{-1}[B]. \tag{S20b}$$

B. Important correct application of the Fourier-transform convention

Many physics equations are derived by assuming that the phase follows $(k_z z - \omega t)$, which implies that the Fourier transform in physics is the inverse Fourier transform in mathematics, i.e., $c_s = 1$. For example in unidirectional pulse propagation equation:

$$\begin{aligned}\partial_z A_p(z,\Omega) = & \, i\left[\beta_p(\omega) - \left(\beta_{(0)} + \beta_{(1)}\Omega\right)\right] A_p(z,\Omega) \\ & + i\frac{\omega n_2}{c}\sum_{\ell mn}\left\{(1-f_R)\, S^K_{p\ell mn}\mathfrak{F}\left[A_\ell A_m A_n^* + \tilde{\Gamma}^K_{p\ell mn}\right\}\right. \\ & \left. + f_R\left\{f_a S^{R_a}_{p\ell mn}\mathfrak{F}\left[A_\ell\left\{h_a(t) * \left[A_m A_n^* + \tilde{\Gamma}^{R_a}_{p\ell mn}\right]\right\}\right] + f_b S^{R_b}_{p\ell mn}\mathfrak{F}\left[A_\ell\left\{h_b(t) * \left[A_m A_n^* + \tilde{\Gamma}^{R_b}_{p\ell mn}\right]\right\}\right]\right\}\right\}, \quad \text{(S21)}\end{aligned}$$

where the explanation of notations can be found in [9]. Its derivation can be found in the supplement of [4] and we can see that A_p results from

$$\vec{\mathbb{E}}(\vec{r},t) = \sum_p \int d\omega \frac{1}{2}\left\{\frac{\vec{F_p}(\vec{r}_\perp,\omega)}{N_p(\omega)} A_p(z,\omega) e^{i[\beta_p(\omega)z - \omega t]} + \text{c.c.}\right\}, \quad \text{(S22)}$$

where A_p represents the envelope of the analytic signal of the real-valued electric field $\vec{\mathbb{E}}(\vec{r},t)$. Some might rewrite it in the time domain (with a narrowband assumption with Taylor-series expansion around center frequency ω_0) as

$$\begin{aligned}\partial_z A_p(z,T) = & \left\{i\left[\beta_p^{(0)}(\omega_0) - \beta^{(0)}\right] - \left[\beta_p^{(1)}(\omega_0) - \beta^{(1)}\right]\partial_T\right\} A_p(z,T) \\ & + i\sum_{m\geq 2}\frac{(i\partial_T)^m}{m!}\beta_p^{(m)}(\omega_0) A_p(z,T) \\ & + \frac{i\omega_0 n_2}{c}\left[1 + \tau_{plmn}\,(i\partial_t)\right]\sum_{lmn}\left\{(1-f_R)\, S^K_{plmn}\left[A_l A_m A_n^* + \tilde{\Gamma}^K_{plmn}\right]\right. \\ & \left. + f_R\left\{f_a S^{R_a}_{plmn}\left[A_l\left\{h_a(t) * \left[A_m A_n^* + \tilde{\Gamma}^{R_a}_{plmn}\right]\right\}\right] + f_b S^{R_b}_{plmn}\left[A_l\left\{h_b(t) * \left[A_m A_n^* + \tilde{\Gamma}^{R_b}_{plmn}\right]\right\}\right]\right\}\right\}, \quad \text{(S23)}\end{aligned}$$

intending to be free from spectral computations. Still, terms with $i\partial_T A(z,T)$ that results from $\Omega A(z,\Omega)$ are related to the convention of Fourier transform with $c_s = 1$:

$$\partial_T A(z,T)\mathfrak{F} - ic_s \Omega A(z,\Omega). \quad \text{(S24)}$$

As a result, it is crucial to apply the correct Fourier-transform convention. In nonlinear optics, it follows the physical convention; i.e., use mathematical (MATLAB's) ifft for Fourier transform into the spectral domain and use mathematical (MATLAB's) fft for inverse Fourier transform into the temporal domain. Some might think that, in numerical computations, the wrong use of Fourier transform simply creates a signal that is a complex conjugate of the correct one, both following the same pulse propagation equation. Since the analytic signal, or its envelope, is generally complex-valued, the spectral signal transformed with mathematical fft is not a complex conjugate of the spectral signal transformed with mathematical ifft. Since $A(z,\Omega)$ is the envelope centering around ω_0 [Fig. S1], the wrong convention represents the field of the reversed frequency sign $A(z,-\Omega)$ that should not follow the same pulse propagation equation as $A(z,\Omega)$. For example, the dispersion term $\beta(\omega)$ should be reversed around ω_0:

$$\beta(\omega = \omega_0 + \Omega) \to \beta(\omega_0 - \Omega). \quad \text{(S25)}$$

In general, a wrong convention of Fourier transform applied to an equation derived with a different convention simply creates a wrong pulse-propagation result, unless the equation is revised accordingly.

C. Conversion of quantities with physical-useful units between FT and DFT

In this section, we derive several formulae for conversion of physical quantities between Fourier transform and discrete Fourier transform.

$$\begin{aligned}\int_{-\infty}^{\infty}|A(t)|^2dt &= \int_{-\infty}^{\infty}C_{\mathfrak{I}\mathfrak{F}}^2\int_{-\infty}^{\infty}\int_{-\infty}^{\infty}A(\omega)A^*(\omega')e^{-ic_s(\omega-\omega')t}d\omega d\omega' dt\\ &= C_{\mathfrak{I}\mathfrak{F}}^2\int_{-\infty}^{\infty}\int_{-\infty}^{\infty}A(\omega)A^*(\omega')\left[\int_{-\infty}^{\infty}e^{-ic_s(\omega-\omega')t}dt\right]d\omega d\omega'\\ &= C_{\mathfrak{I}\mathfrak{F}}^2\int_{-\infty}^{\infty}\int_{-\infty}^{\infty}A(\omega)A^*(\omega')\left[2\pi\delta(c_s(\omega-\omega'))\right]d\omega d\omega'\\ &= 2\pi C_{\mathfrak{I}\mathfrak{F}}^2\int_{-\infty}^{\infty}|A(\omega)|^2d\omega,\quad \delta(c_s(\omega-\omega')) = \frac{\delta(\omega-\omega')}{|c_s|} = \delta(\omega-\omega')\\ &= \frac{C_{\mathfrak{I}\mathfrak{F}}}{C_{\mathfrak{F}}}\int_{-\infty}^{\infty}|A(\omega)|^2d\omega.\quad \because C_{\mathfrak{I}\mathfrak{F}} = \frac{1}{2\pi C_{\mathfrak{F}}}\end{aligned} \tag{S26}$$

Eq. (S26) leads to the general formulation of the Parseval's theorem:

$$\frac{1}{C_{\mathfrak{I}\mathfrak{F}}}\int_{-\infty}^{\infty}|A(t)|^2dt = \frac{1}{C_{\mathfrak{F}}}\int_{-\infty}^{\infty}|A(\omega)|^2d\omega. \tag{S27}$$

With Eq. (S16) and $\Delta\omega = \frac{2\pi}{\mathfrak{N}\Delta t}$, we can derive the discrete version of the Parseval's theorem:

$$\frac{1}{C_{\mathfrak{I}\mathfrak{F}_D}}\sum_{n=1}^{\mathfrak{N}}|A(t_n)|^2 = \frac{1}{C_{\mathfrak{F}_D}}\sum_{m=1}^{\mathfrak{N}}|A_D(\omega_m)|^2. \tag{S28}$$

Rewriting the Parseval's theorem in powers leads to $\int_{-\infty}^{\infty}P(t)dt = \int_{-\infty}^{\infty}P(\omega)d\omega$, where $P(t) = |A(t)|^2$. Since $P(t)$ has the unit of "$\mathrm{W} = \mathrm{J/s}$," $P(\omega) = \frac{C_{\mathfrak{I}\mathfrak{F}}}{C_{\mathfrak{F}}}|A(\omega)|^2 = \frac{1}{2\pi C_{\mathfrak{F}}^2}|A(\omega)|^2$ has the unit of "$\mathrm{J/(rad\cdot Hz)}$" [ω has a unit of "$\mathrm{Hz}/(2\pi) = \mathrm{rad\cdot Hz}$"]. To calculate the spectrum with the unit of "$\mathrm{J/Hz}$" numerically,

$$P(\nu) = 2\pi P(\omega) = \frac{1}{C_{\mathfrak{F}}^2}|A(\omega)|^2 = \left(\frac{\Delta t}{C_{\mathfrak{F}_D}}\right)^2|A_D(\omega)|^2, \tag{S29}$$

by applying Eq. (S16) and $C_{\mathfrak{F}}C_{\mathfrak{I}\mathfrak{F}} = \frac{1}{2\pi}$. $\int P(\omega)d\omega = \int P(\nu)d\nu$ leads to $P(\nu) = 2\pi P(\omega)$. With the DFT convention we use here ($C_{\mathfrak{F}_D} = \frac{1}{\mathfrak{N}}$), it becomes $P(\nu) = (T^w)^2|A_D(\omega)^2|$.

The Parseval's theorem assumes the unit of energy (J) after the integral. However, for continuous waves, a unit in terms of *power* makes more sense in the frequency domain. With a known time window $T^w = \mathfrak{N}\Delta t$, the continuous-wave spectral energy in this time window is $P_{\mathrm{CW}}(\omega)T^w = \frac{1}{2\pi C_{\mathfrak{F}}^2}|A_{\mathrm{CW}}(\omega)|^2$, where $P_{\mathrm{CW}}(\omega)$ is in "$\mathrm{W/(rad\cdot)Hz}$." Hence,

$$|A_{\mathrm{CW}}(\omega)| = C_{\mathfrak{F}}\sqrt{2\pi P_{\mathrm{CW}}(\omega)T^w} = C_{\mathfrak{F}}\sqrt{P_{\mathrm{CW}}(\nu)T^w}, \tag{S30}$$

by use of the relation $P_{\mathrm{CW}}(\nu) = 2\pi P_{\mathrm{CW}}(\omega)$. $P_{\mathrm{CW}}(\nu)$ is in $\mathrm{W/Hz}$. This leads to, with Eq. (S16),

$$|A_{D,\mathrm{CW}}(\omega)| = \frac{C_{\mathfrak{F}_D}}{\Delta t}\sqrt{2\pi P_{\mathrm{CW}}(\omega)T^w} = \frac{C_{\mathfrak{F}_D}}{\Delta t}\sqrt{P_{\mathrm{CW}}(\nu)T^w}, \tag{S31}$$

which results in $|A_{D,\mathrm{CW}}(\omega)| = \sqrt{P_{\mathrm{CW}}(\nu)/T^w} = \sqrt{P_{\mathrm{CW}}(\nu)\Delta\nu}$ with the DFT convention we use here (note that $T^w = 1/\Delta\nu$).

In the common model of adding noise photon (e.g., shot noise), the noise is added as a CW background with one noise photon per frequency mode/bin, or equivalently, with an one-noise-photon spectral distribution ($\mathrm{J = W/Hz}$) $P_{\mathrm{noise}}(\nu) = h\nu$ [10][11][12][13]. Eq. (S30) leads to

$$|A_{\text{noise photon}}(\omega)| = C_{\mathfrak{F}}\sqrt{T^w h\nu} \tag{S32a}$$

$$|A_{D,\text{noise photon}}(\omega)| = \frac{C_{\mathfrak{F}_D}}{\Delta t}\sqrt{T^w h\nu}, \tag{S32b}$$

Eq. (S32b) gives $|A_{D,\text{noise photon}}(\omega)| = \sqrt{h\nu/T^w} = \sqrt{h\nu\Delta\nu}$ with the DFT convention we use here.

The power spectral density $P(\omega)$ or $P(\nu)$ can also be represented in the wavelength domain. First, we derive the relation

$$\begin{aligned} c &= \nu\lambda \\ \Rightarrow 0 &= \lambda d\nu + \nu d\lambda \\ \Rightarrow d\nu &= -\frac{\nu}{\lambda}d\lambda = -\frac{c}{\lambda^2}d\lambda \end{aligned} \tag{S33}$$

which leads to

$$\begin{aligned} \int P(\lambda)|d\lambda| &= \int P(\nu)d\nu \\ &= \int P(\nu)|-\frac{c}{\lambda^2}d\lambda| = \int \frac{c}{\lambda^2}P(\nu)|d\lambda| \\ &\Rightarrow P(\lambda) = \frac{c}{\lambda^2}P(\nu) \end{aligned} \tag{S34}$$

Because wavelength and frequency have an inverse relation, and the power is always positive, an absolute value is taken in derivation. $P(\lambda)$ has the unit "$\mathrm{J/m}$," whose CW version [Eqs. (S30) and (S31)] is in "$\mathrm{W/m}$."

3. Discrete Fourier transform (DFT)

In practice, DFT is computed with finite sampling in a finite window. If a signal is temporally-confined [Fig. S2(a)], the integration range of Fourier transform can be changed from $(-\infty, \infty)$ to a small window that is just sufficiently large to cover the signal, which is practically realizable with DFT. However, in general, DFT does not necessarily duplicate the Fourier transform because finite-sampling DFT discards the signal information beyond the window. For example, the DFT of a known temporal signal remains the same for $\omega \to \omega + 2\pi\nu^w$:

$$\begin{aligned} A(\omega + 2\pi\nu^w) = \mathfrak{F}_D[A(t_n)] &\equiv C_{\mathfrak{F}_D}\sum_{n=1}^{\mathfrak{N}} A(t_n)e^{ic_s(\omega+2\pi\nu^w)t_n} \\ &= A(\omega),\ \because t_n\nu^w = n, \end{aligned} \tag{S35}$$

where ν^w is the frequency window. The formulation of DFT establishes the implicit periodicity of the transformed signal [Fig. S2(b)]. Due to the symmetry in formulation of DFT and inverse DFT, the implicit periodicity is established for both the temporal and spectral signals, or the spatial and $\vec{k}_\perp$ signals.

doi.org/10.32388/JFPRSL.2

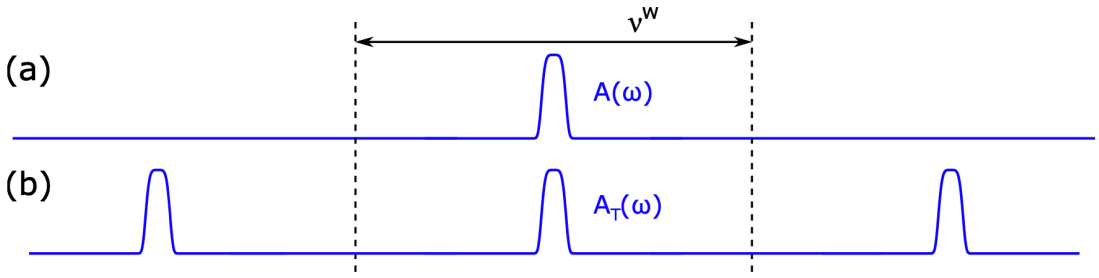

Figure S2. (a) Spectrally-confined signal. A frequency window ν^w covers the signal. (b) Spectrally-periodic signal with a period ν^w.

3.1. fftshift/ifftshift and phase unwrapping

During operations of DFT in numerical computations, it is sometimes necessary to apply (MATLAB's) "fftshift" and "ifftshift," the offset of the signal. For example, because the frequency coordinate of the spectral field calculated from DFT has zero frequency at the first sampling point (the left edge of the frequency window), the spectrum appears as split into half, one at the left edge and the other at the right edge (Fig. S3). This occurs due to DFT's assumed periodicity of the spectral field. It is then desirable to "shift" the signal to the center of the window for visualization or other computations. Despite various conventions, fftshift is used to shift the signal to the center of the window (move $t_x = 0$ or $\nu_x = 0$ to window's center), whether it is in temporal or spectral domain. On the other hand, ifftshift is to cancel the fftshift effect and shifts the signal to center at $t_x = 0$ or $\nu_x = 0$ (left edge of the window). t_x and ν_x represent the sampling coordinates in the temporal and spectral domains, respectively. They should not be used simply as a pair of (fft,fftshift) and (ifft, ifftshift) due to different Fourier-transform conventions. For example, to compute the spectrum under the physical Fourier-transform convention ($c_s = 1$), we should follow (in MATLAB syntax below)

```
Nt = size(field,1); % the number of sampling points
t = (-Nt/2:Nt/2-1)'*dt; % ps; time coordinates; dt = temporal sampling spacing
c = 299792.458; % nm/ps; speed of light
f = f0+(-Nt/2:Nt/2-1)'/(Nt*dt); % THz; frequency coordinate; f0 = center frequency of the freuqnency window
wavelength = c./f; % nm
correct_unit = (Nt*dt)^2/1e3; % to make the spectrum of the correct unit "nJ/THz" [Eq.(S29)]
                              % "/1e3" is to make pJ into nJ
                              % "field" unit: sqrt(W)
spectrum = abs(fftshift(ifft(field),1)).^2*correct_unit; % nJ/THz; centered at the frequency window [Fig.S2(c)]
```

In practice, the time coordinate is placed such that the pulse at the center of the numerical time window locates at $t = 0$ in real-time (t) coordinates [Fig. S3(b)]. Do not confuse it with the pulse locating at $t_x = 0$ [Fig. S3(a)]. In principle, the time coordinate can be placed arbitrarily because numerical computations see only the sampling-point coordinate t_x or ν_x.

doi.org/10.32388/JFPRSL.2

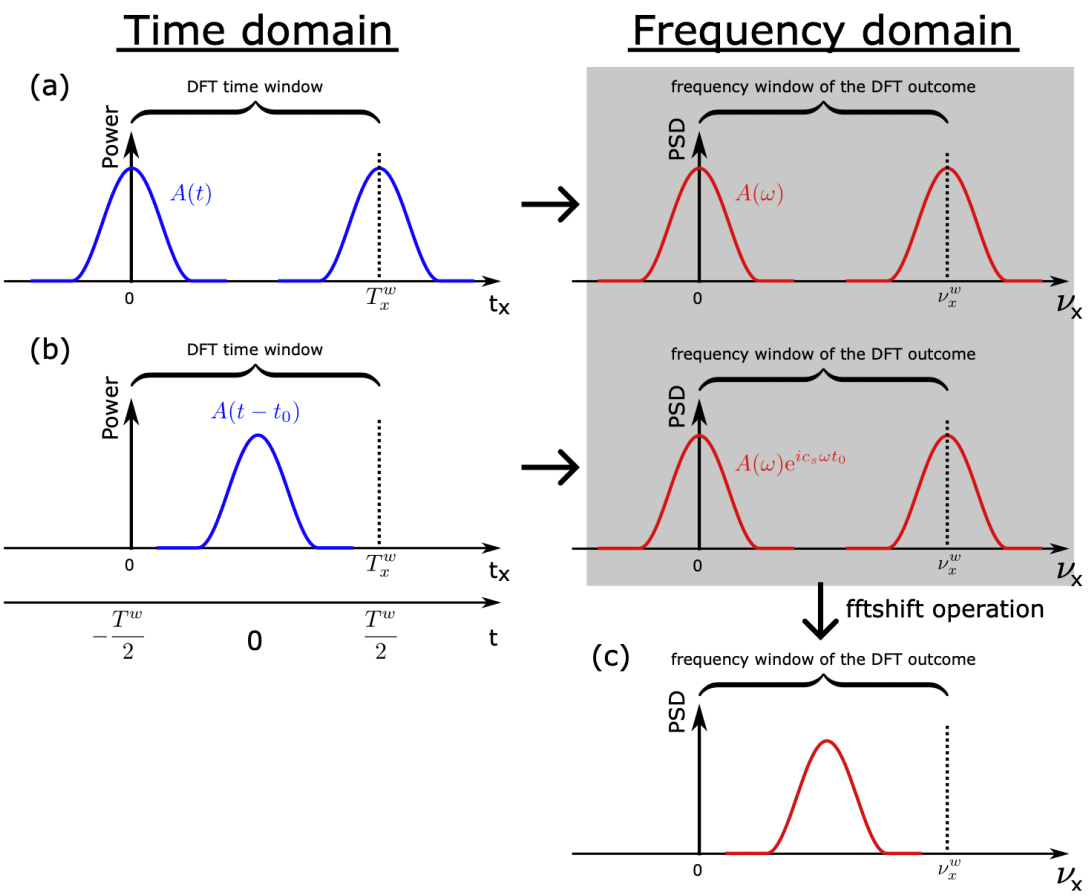

Figure S3. DFT conversion. (a) is the "formal" use of DFT when the temporal profile $|A(t)|^2$ is centered at $t = 0$. However, in numerical simulations, it is common to place the pulse at the center of the time window for visualization purpose (b), resulting in a spectral phase shift that doesn't affect the spectral shape. (c) is the result after fftshift centers the spectrum with respect to the frequency window. PSD: power spectral density $\sim |A(\omega)|^2$. Here, the subscript "x" represents the coordinate of sampling points, rather than the actual time and frequency coordinates.

Due to the numerical phase-unwrapping process, the temporal position of the pulse can affect the acquisition of a smooth phase relation $\phi(\omega)$. Numerically, phase of a complex number is found within the range of either $(0, 2\pi]$ or $(-\pi, \pi]$. Phase unwrapping is a process that removes the phase jump by adding multiples of $\pm 2\pi$ when the phase change between two data points is larger than a threshold value, typically π[Fig. S4(a)]. This operation is crucial in phase computations, such as characterizing the second-order spectral phase $\phi\omega^2$ in a pulse to determine the pulse-dechirping strategy (see Sec. 4). Therefore, it is important to unwrap the phase correctly such that it does not arbitrarily add multiples of $\pm 2\pi$ that distorts the phase relation $\phi(\omega)$. Phase unwrap can go wrong when the phase relation $\phi(\omega)$ changes too drastically beyond the threshold value. The unwrapping operation will attempt to reduce the variation, leading to a kink, followed by a slope of reverse sign due to continuous reduction of phase change by $\pm 2\pi$ [Fig. S4(b)]. Since a temporal offset of a pulse adds a linear spectral phase $(c_s\omega t_0)$ [Fig. S3(b)], this extra addition might increase the rate of phase change and trigger the wrong unwrapping operation. As a result, in ultrafast optics, the fundamental principle is to

doi.org/10.32388/JFPRSL.2

first remove the temporal offset and place the pulse at $t_x = 0$ (left edge of the time window), as in Fig. S3(a), before applying any spectra-phase computations. The value of temporal offset is remembered to recover the pulse position after the operation if necessary. However, if the phase relation inherently shows a rapid phase change, as illustrated in Fig. S4(b), the only viable solution to accurately unwrap the phase is to enhance the spectral resolution, which necessitates extending the numerical time window.

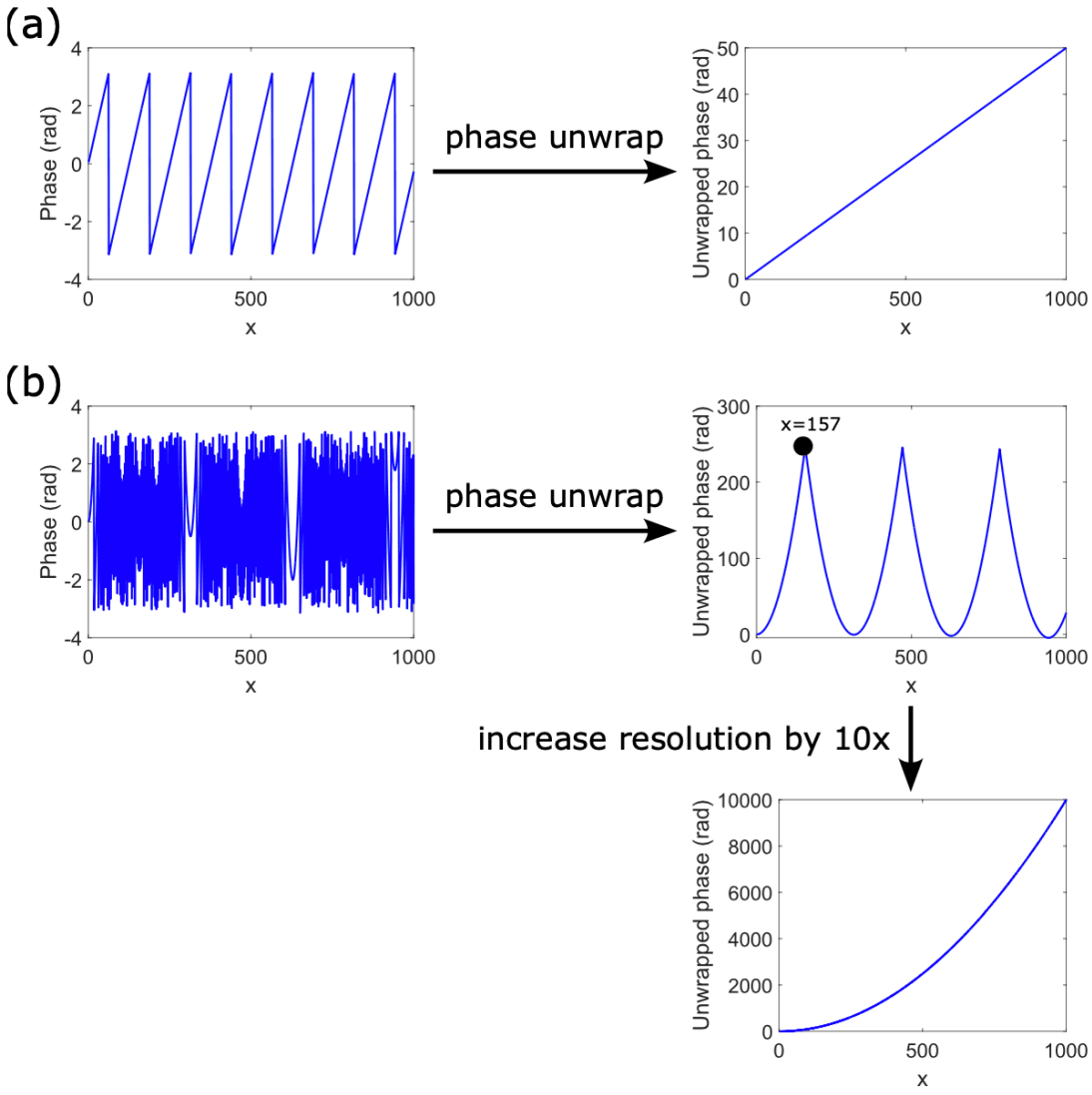

Figure S4. Phase-unwrapping process: $\phi(x) = \text{unwrap}(\text{angle}(y(x)))$ ($x = 0:1:1000$ here, integer array from 0 to 1000 in MATLAB syntax). In MATLAB, phase from $\text{angle}(\cdot)$ is in $(-\pi, \pi]$. (a) Linear spectral phase: $y = e^{ix/20}$. Its phase does not vary dramatically between data points, so phase is correctly unwrapped. (b) Quadratic spectral phase: $y = e^{ix^2/100}$. This phase rapidly varies for larger values of x. Beyond $x = 157$, the phase change between two consecutive points always exceeds π, constantly triggering phase-unwrapping operation to add another -2π. This results in decreasing phase values, ultimately leading to the formation of multiple parabolic curves. To correctly unwrap the phase, the resolution is increased to 10 times: $x = 0:0.1:1000$ (from 0 to 1000 with 0.1 spacing).

doi.org/10.32388/JFPRSL.2

DFT's convolution

In ultrafast optics, convolution is commonly used. There are two types of convolutions:

$$\text{linear convolution: } (A*B)(t) \equiv \int_{-\infty}^{\infty} A(\tau)B(t-\tau)d\tau \tag{S36a}$$

$$\text{circular convolution: } (A_T*B_T)_{\text{circular}}(t) \equiv \int_{t_0}^{t_0+T} A_T(\tau)B_T(t-\tau)d\tau. \tag{S36b}$$

with A_T and B_T being periodic with period T, and t_0 is an arbitrary value. Both satisfy similar convolution theorems:

$$\text{linear convolution theorem: } \mathfrak{F}[A*B] = \frac{1}{C_{\mathfrak{F}}}\mathfrak{F}[A]\mathfrak{F}[B] \tag{S37a}$$

$$\text{circular convolution theorem: } \mathfrak{F}_T[(A_T*B_T)_{\text{circular}}] = \frac{1}{C_{\mathfrak{F}}}\mathfrak{F}_T[A_T]\mathfrak{F}_T[B_T], \tag{S37b}$$

where $\mathfrak{F}_T[A_T] = C_{\mathfrak{F}}\int_{t_0}^{t_0+T} A_T(t)e^{ic_s\omega t}dt$ is the modified Fourier transform with a small integration range T. In practical numerical computations, it is required to define a window that covers the signal and decide the sampling conditions (uniform vs. non-uniform sampling, sampling spacing, and the number of sampling points), which leads to finite number of sampling points within a finite window. Therefore, the linear convolution theorem in Eq. (S37a), which needs an infinite integration range $(-\infty,\infty)$ and thus an infinite number of sampling points, is never numerically useful. On the other hand, the circular convolution theorem is useful, which can be easily computed with the (finite-sampling) fast-Fourier-transform (fft)-based DFT that offers significant computational efficiency. However, in physics equations, the convolution is always the "linear" convolution. Only under specific conditions do the two convolutions become equivalent, allowing us to solve the "linear" convolution with the computationally-efficient circular convolution theorem.

Circular (or cyclic) convolution arises from the linear convolution involving a (or two) periodic signal [Fig.S5(b)]:

$$\begin{aligned}
(A*B_T)(t) &\equiv \int_{-\infty}^{\infty} A(\tau)B_T(t-\tau)d\tau, \quad B_T \text{ is periodic with period } T \\
&= \sum_{k=-\infty}^{\infty}\int_{t_0}^{t_0+T} A(\tau'+kT)B_T(t-\tau'-kT)d\tau' = \sum_{k=-\infty}^{\infty}\int_{t_0}^{t_0+T} A(\tau'+kT)B_T(t-\tau')d\tau' \\
&= \int_{t_0}^{t_0+T}\left(\sum_{k=-\infty}^{\infty} A(\tau'+kT)\right)B_T(t-\tau')d\tau' \\
&= \int_{t_0}^{t_0+T} A_T(\tau')B_T(t-\tau')d\tau', \quad A_T = \sum_{k=-\infty}^{\infty} A(\tau'+kT) \text{ is periodic with period } T \\
&\equiv (A_T*B_T)_{\text{circular}}(t).
\end{aligned} \tag{S38}$$

Furthermore, if $t\in[t_0,t_0+T]$ which $\mathfrak{F}_T^{-1}$ is defined to recover to, it can be calculated with

$$(A_T*B_T)_{\text{circular}} = \mathfrak{F}_T^{-1}\left[\frac{1}{C_{\mathfrak{F}}}\mathfrak{F}_T[A_T]\mathfrak{F}_T[B_T]\right] \tag{S39}$$

due to the circular convolution theorem, which can be computed with the finite-sampling DFT.

Only under limited conditions is discrete linear convolution theorem [Eq. (S17); discrete version of Eq (S37a)] practically numerically available, i.e., with finite sampling points in a limited (temporal/spectral/spatial) range. For signals that are confined in time [Fig. S5(a)], the integration range of linear convolution [Eq. (S36a)] can be significantly reduced from $(-\infty,\infty)$ to a finite range T^w that covers the signals. Because linear convolution can be visualized with integration of A and a sliding t-inverted B (whose amount of sliding is determined by C's coordinate), the approximate width of the

convoluted signal C is the summation of widths of A and B: $\Delta t_C = \Delta t_A + \Delta t_B$. Therefore, the condition to satisfy to avoid a distorted convolution is $T^w \geq \Delta t_C$, which, in the discrete manner, becomes $T^w \geq \Delta t_C = \mathfrak{N}_A + \mathfrak{N}_B - 1$ [$\mathfrak{N}_i$ is the number of points of signal i ($i = A, B$)]. With finite discrete sampling, the continuous Fourier transform and inverse Fourier transform within the reduced range T^w can be, respectively, numerically computed with fft-based DFT and inverse DFT, which leads to efficient computation of the discrete linear convolution theorem.

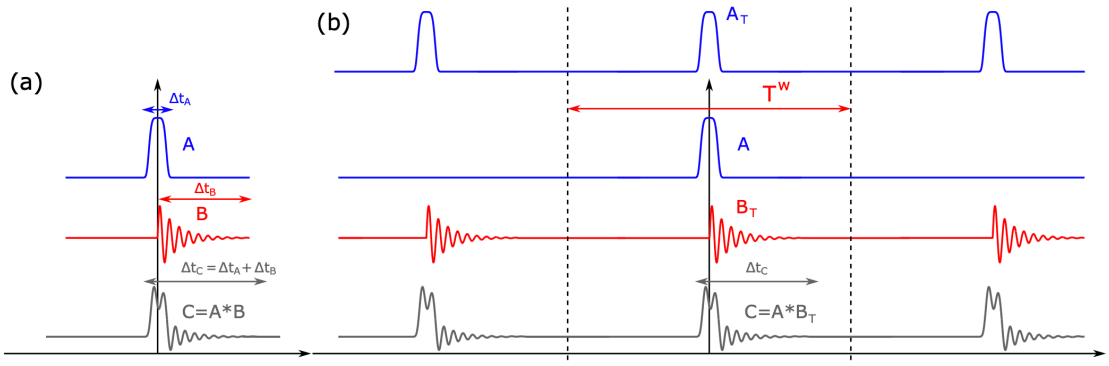

Figure S5. Linear convolution $C = A * B$. (a) is the convolution scheme when signals A and B are confined in time. (b) is the scheme when B becomes a periodic signal with period T^w.

The DFT-based convolution theorem [Eq. (S17a)]

$$A * B = \mathfrak{F}_D^{-1}\left[\frac{\Delta t}{C_{\mathfrak{F}}}\mathfrak{F}_D[A]\mathfrak{F}_D[B]\right] \tag{S40}$$

implicitly assumes periodicity for the convoluted signal $(A * B)$ due to $\mathfrak{F}_D^{-1}$. The periodicity in convolution implies periodicity in either signal A or signal B, or both. This establishes equivalence between the DFT-based convolution theorem [Eq. (S40)] and the circular convolution theorem [Eq. (S37b)]. In conclusion, the practical finite-sampling (with a finite range) DFT-based convolution theorem is applicable to confined signals or periodic signals.

It is important to note that the discussion here applies to inverse-Fourier-transform-based convolution theorems (with $\mathfrak{F} \leftrightarrow \mathfrak{F}^{-1}$ or $\mathfrak{F}_D \leftrightarrow \mathfrak{F}_D^{-1}$) [Eqs. (S10b) and (S17b)], or the spectral (or $\mathbf{k}_\perp$) domain (with $t \leftrightarrow \nu$ or $\mathbf{r}_\perp \leftrightarrow \mathbf{k}_\perp$), due to the symmetric formulation of the Fourier-transform pair.

In ultrafast optics, there are situations when the pulse is short but the Raman response to be convoluted with extends in time [Fig. S6(a) with an extended signal B]. Since only the physical phenomena of the pulse matters, it is desirable to compute the convolution with a window that is comparable to the pulse width [Fig. S6(b)]. However, the small time window clips the extended signal, resulting in a distorted convoluted outcome. Because the width of the convoluted signal Δt_C is larger than the clipped extended signal Δt_B, there is a width of $\Delta t_C - \Delta t_B = \Delta t_A$ of distortion. If Δt_B is too small due to significant clipping, the distortion happens inside the time window. By temporally shifting the extended signal B such that it is clipped less (it is still the same function $B(t)$ but is shifted with respect to numerical sampling points), the valid part of the convolution increases so that the entire convoluted signal in the time window is valid [Fig. S6(c)]. Due to the assumed periodicity resulting from the DFT-based convolution theorem, it is important to have a

doi.org/10.32388/JFPRSL.2

window that covers the convoluted signal; otherwise, there will be distortion due to overlapped convoluted signals [Fig. S6(d)]. Zero-padding is an efficient solution to extend the window [see MATLAB code below; Fig. S6(e)]. Since the convoluted signal has a width of Δt_C, both signals are extended to a width larger than $\Delta t_C = \mathfrak{N}_A + \mathfrak{N}_B - 1$ from their original widths ($\Delta t_A = \mathfrak{N}_A$ or $\Delta t_B = \mathfrak{N}_B$). After convolution (with the DFT-based convolution theorem) with zero-padded signals, only those in the original time window are kept, which is the valid part of the convoluted signal.

```
% For example,
A = (1:5)';
B = rand(10,1);

Na = length(A);
Nb = length(B);
Nc = Na + Nb - 1; % length of the convoluted signal

% A and B are column vectors here
A = [A;zeros(Nc-Na,1)]; % zero-padding
B = [B;zeros(Nc-Nb,1)]; % zero-padding
C = Nc*fft(ifft(A).*ifft(B)); % Eq.(S40) but dt is ignored here

% C equals conv(A,B).
```

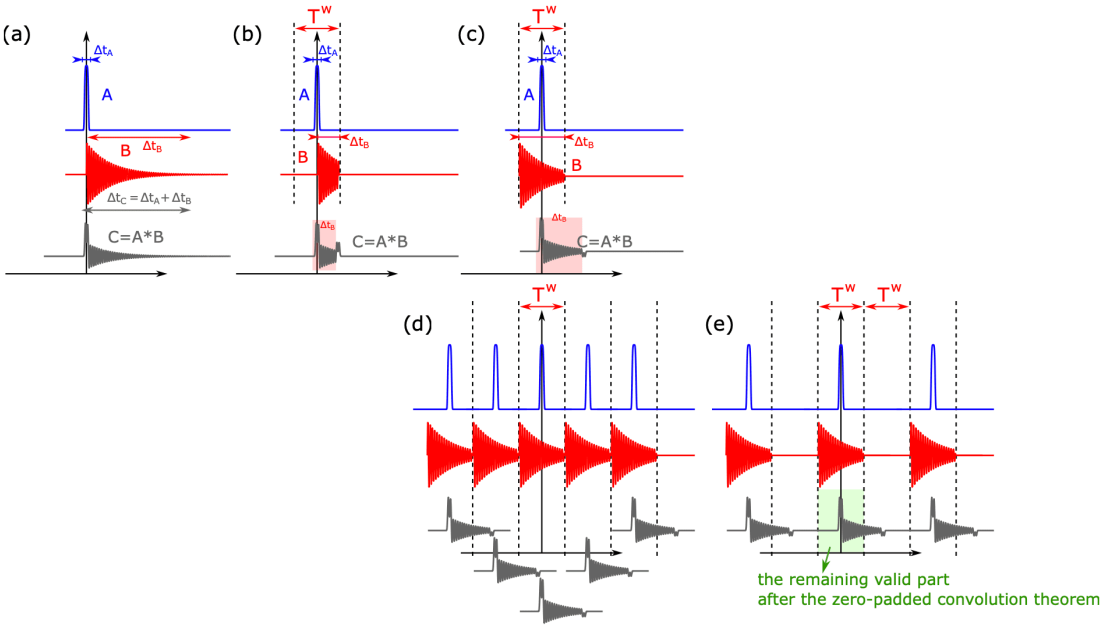

Figure S6. (a) Linear convolution of A with a temporally-extended B. (b) and (c) are the convolutions with B clipped beyond the window T^w, with a shifted B in (c). (d) and (e) are convolution results without and with zero-padded signals, respectively. Convoluted signals in (d) from each window/period overlap, distorting the outcome, while zero-padding avoids the distortion from overlapping.

4. Phenomena with complex-valued Fourier transform

Figs. S7 and S9 show how the phase affects the signal. When the pulse has a flat phase in time domain, it is called "a transform-limited pulse." Its temporal and spectral width satisfy a fixed time-bandwidth product: a more-broadband pulse has a smaller duration. By adding a temporally (or spectrally) varying phase to the pulse, it modulates the signal.

doi.org/10.32388/JFPRSL.2

For example, adding a parabolic (second-order) phase to the temporal profile of a transform-limited signal creates a chirp, i.e., varying frequency at different temporal slices, broadening the spectrum [Fig. S7(b)]. The temporal frequency change follows $\Delta\omega(t) = \frac{1}{-c_s}\phi t(t)$, so the phase effect to the signal is also dependent on the convention of Fourier transform. Similarly, adding a parabolic phase to the spectral profile increases the pulse duration, which is the "dispersion" effect: different frequencies moves at different speeds for a certain distance, widening the pulse's temporal profile [Figs. S7(c) and S8]. Fig. S9 shows the effect of a cubic phase, which broadens the spectral [Fig. S9(b)] or temporal [Fig. S9(c)] profiles with pedestals. Adding a linear chirp to the pulse to increase the pulse duration [Fig. S7(c)], reducing the peak power, is the basis of the chirp-pulse amplification[14] that was awarded the Nobel Prize in Physics in 2018. It enables amplification of an ultrashort pulse without suffering from significant nonlinear-phase accumulations due to a reduced peak power.

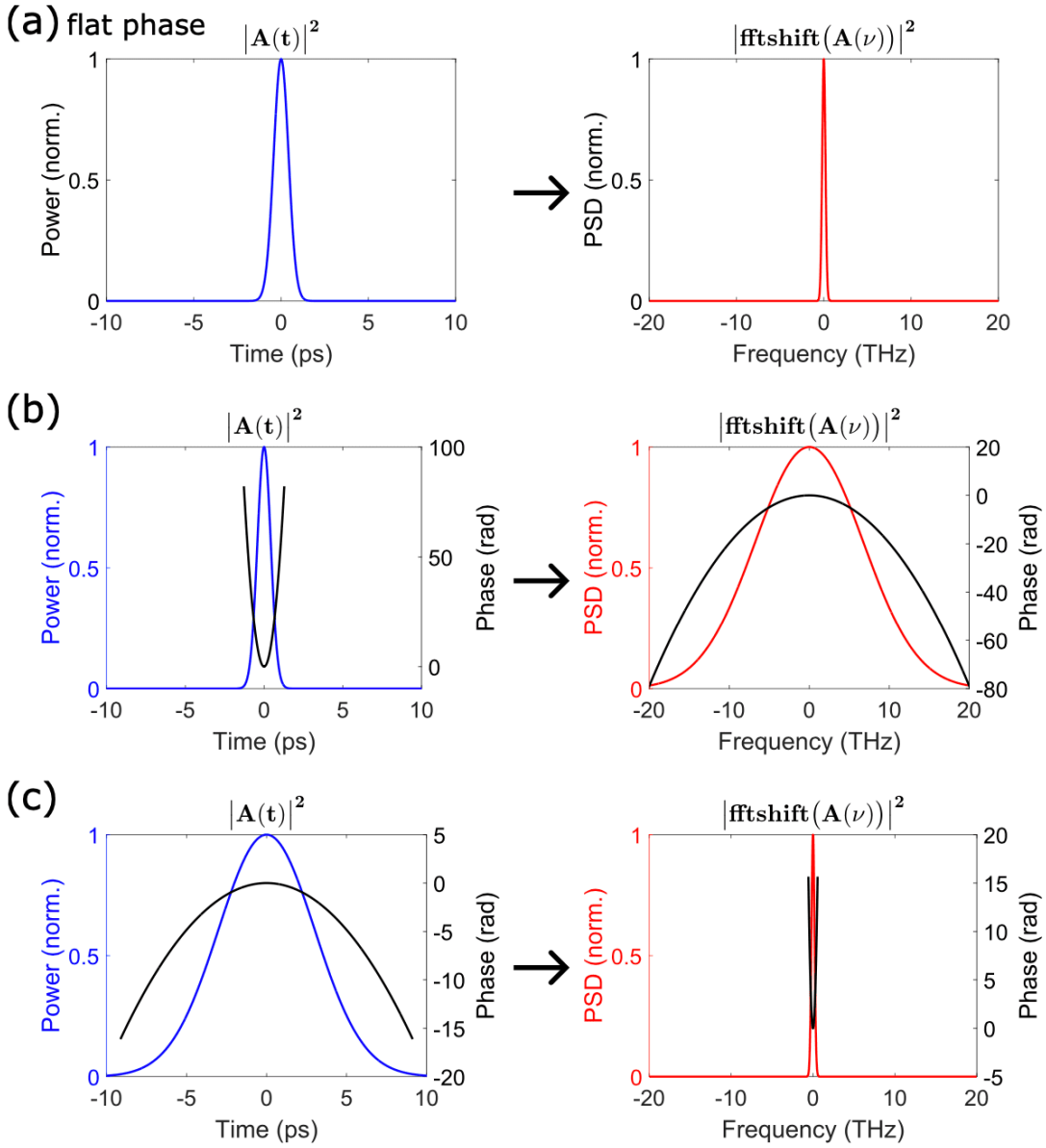

Figure S7. DFT conversion of a second-order chirped signal. (a) transform-limited pulse that has only flat phase in time domain. (b) and (c) add a parabolic phase to the temporal and spectral profiles, respectively.

doi.org/10.32388/JFPRSL.2

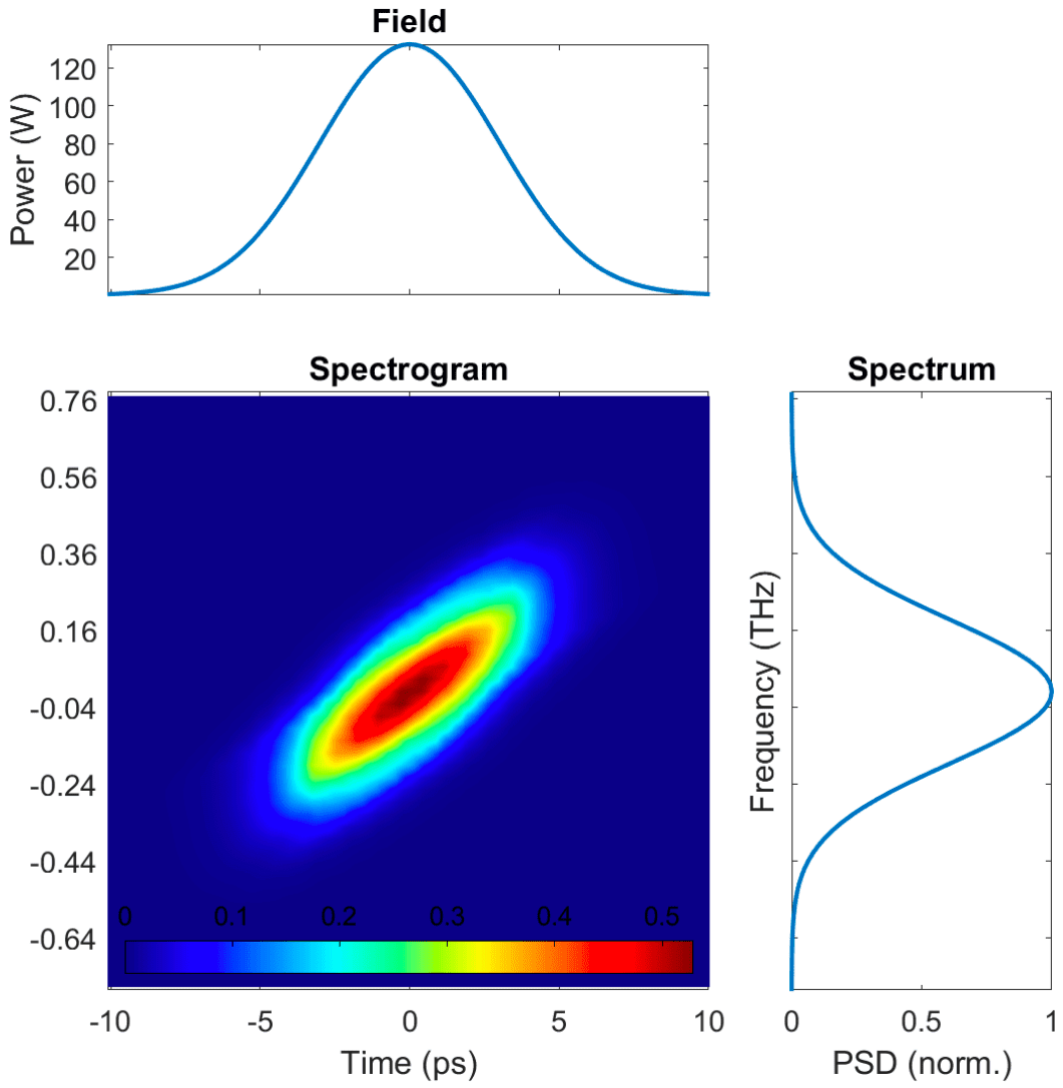

Figure S8. Spectrogram of a parabolically-chirped signal [Fig. S7(c)]. Here, the signal is positively-chirped such that lower-frequency components are in the temporal leading edge.

doi.org/10.32388/JFPRSL.2

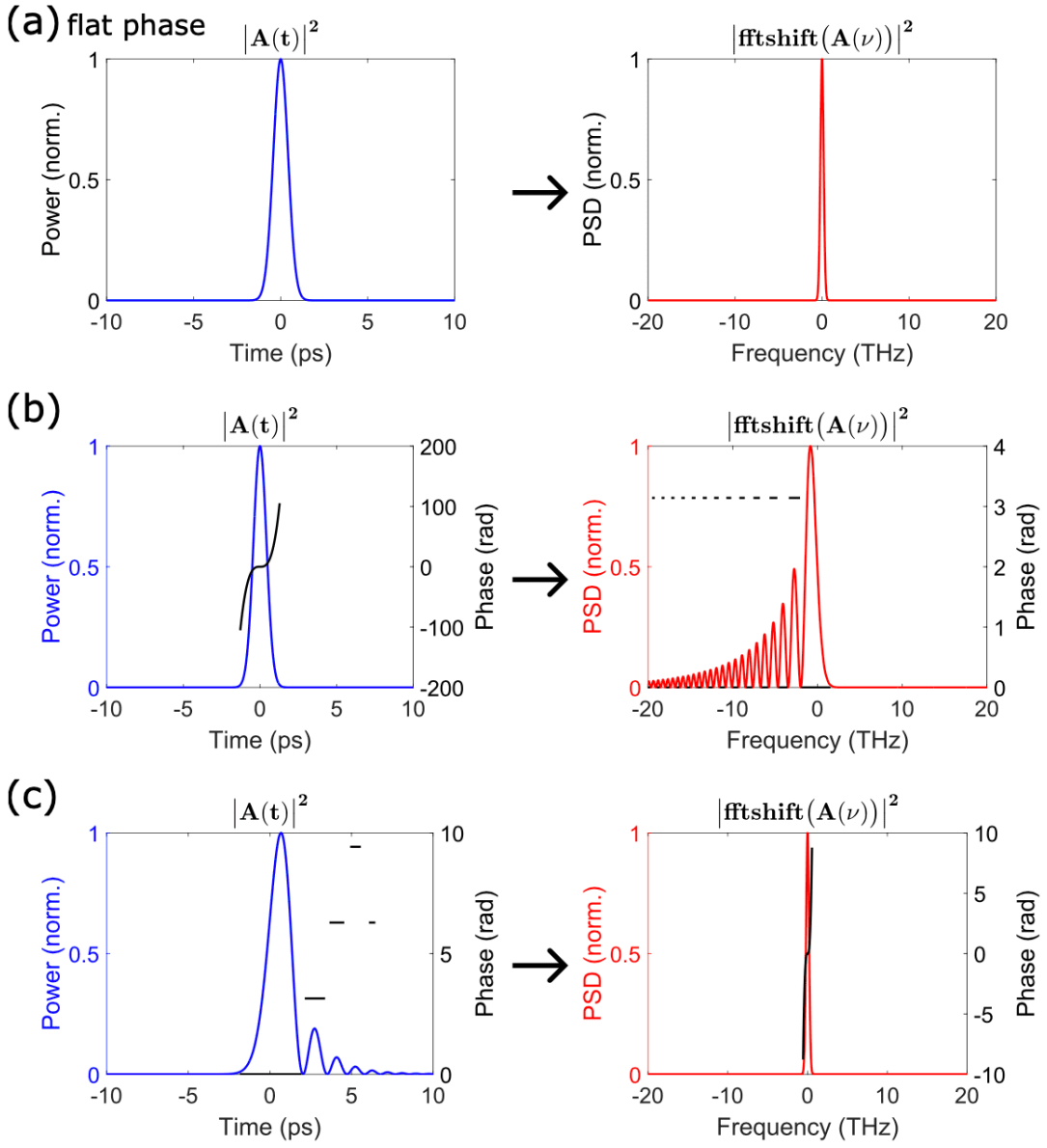

Figure S9. DFT conversion of a third-order chirped signal. (a) transform-limited pulse that has only flat phase in time domain. (b) and (c) add a cubic phase to the temporal and spectral profiles, respectively.

5. Hankel transform: 2D spatial Fourier transform of $A(r)$

In scenarios that require a full-field, instead of mode-resolved, simulation, pulse propagation most likely exhibits radial symmetry, such as in a multipass cell[15][16] and a multiplate compressor[17][18][19]. Hankel transform is the core element of computations of such radially-symmetric system, which we will introduce in this section.

doi.org/10.32388/JFPRSL.2

A. Introduction

During solving the full-field pulse propagation equation, the Hankel transform $\mathfrak{H}$ emerges from the two-dimensional "spatial" Fourier transform $\mathfrak{F}_{k_\perp} = \mathfrak{F}_x\mathfrak{F}_y$ of a radially-symmetric function:

$$\begin{aligned}
A(k_\perp) = \mathfrak{F}_{k_\perp}[\![A(\vec{r}_\perp = \vec{r}_\perp)]\!] &\equiv C_{\mathfrak{F}}^2 \int_{-\infty}^{\infty}\int_{-\infty}^{\infty} A(r_\perp) e^{ic_s(k_x x + k_y y)}\, dxdy \\
&= C_{\mathfrak{F}}^2 \int_0^{2\pi}\int_0^{\infty} A(r_\perp) e^{ic_s|\vec{k}_\perp||\vec{r}_\perp|\cos\theta} |\vec{r}_\perp| d|\vec{r}_\perp| d\theta \quad , \ \vec{k}_\perp \cdot \vec{r}_\perp = |\vec{k}_\perp||\vec{r}_\perp|\cos\theta \\
&= C_{\mathfrak{F}}^2 \int_0^{\infty} A(r_\perp)|\vec{r}_\perp| \left(\int_0^{2\pi} e^{ic_s|\vec{k}_\perp||\vec{r}_\perp|\cos\theta} d\theta\, d|\vec{r}_\perp| \right. \\
&= 2\pi C_{\mathfrak{F}}^2 \int_0^{\infty} A(r_\perp) J_0(|c_s|k_\perp r_\perp) r_\perp dr_\perp \\
&\equiv 2\pi C_{\mathfrak{F}}^2 \mathfrak{H}[\![A]\!](k_\perp) \quad \because |c_s| = 1,
\end{aligned} \tag{S41}$$

where $J_0(z) = \frac{1}{2\pi}\int_0^{2\pi} e^{iz\cos\theta} d\theta$ is employed. Notations are simplified with $k_\perp = |\vec{k}_\perp| = |(k_x, k_y)|$ and $r_\perp = |\vec{r}_\perp| = |(x, y)|$. Similarly, the inverse Fourier transform becomes

$$\begin{aligned}
A(r_\perp) = \mathfrak{F}_{k_\perp}^{-1}[\![A(k_\perp)]\!] &\equiv C_{\mathfrak{IF}}^2 \int_{-\infty}^{\infty}\int_{-\infty}^{\infty} A(k_\perp) e^{-ic_s(k_x x + k_y y)} dk_x dk_y \\
&= 2\pi C_{\mathfrak{IF}}^2 \int_0^{\infty} A(k_\perp) J_0(|c_s|k_\perp r_\perp) k_\perp dk_\perp \\
&\equiv 2\pi C_{\mathfrak{IF}}^2 \mathfrak{H}^{-1}[\![A]\!](k_\perp).
\end{aligned} \tag{S42}$$

The minus sign in the exponent disappears due to the integral over a full 2π angle; as a result, the Hankel transform displays the same formulation whatever the Fourier-transform convention is. In general, Hankel transform is defined for $\nu \geq -1/2$; however, because we are more interested in using it to solve radially-symmetric systems, discussion is limited only to Hankel transform of order 0 (i.e., $\nu = 0$). The Hankel transform of order 0 is defined as

$$\begin{aligned}
A_H(k_\perp) = \mathfrak{H}[A(r_\perp)] &\equiv \int_0^{\infty} A(r_\perp) J_0(k_\perp r_\perp) r_\perp dr_\perp \\
A(r_\perp) = \mathfrak{H}^{-1}[A_H(k_\perp)] &\equiv \int_0^{\infty} A_H(k_\perp) J_0(k_\perp r_\perp) k_\perp dk_\perp .
\end{aligned} \tag{S43}$$

With the orthogonality relation

$$\int_0^{\infty} J_\nu(kr) J_\nu(k'r) r dr = \frac{\delta(k-k')}{k}, \quad k, k' > 0, \tag{S44}$$

Eq. (S43) forms a Hankel-transform pair with $\mathfrak{H}\mathfrak{H}^{-1} = \mathfrak{H}^{-1}\mathfrak{H} = 1$. This relation can also be verified with one-dimensional $\mathfrak{F}\mathfrak{F}^{-1} = \mathfrak{F}^{-1}\mathfrak{F} = 1$ by noting that $C_{\mathfrak{F}}C_{\mathfrak{IF}} = \frac{1}{2\pi}$ with the following Fourier-transform representation:

$$\mathfrak{F}_{k_\perp} = 2\pi C_{\mathfrak{F}}^2 \mathfrak{H} \tag{S45a}$$
$$\mathfrak{F}_{k_\perp}^{-1} = 2\pi C_{\mathfrak{IF}}^2 \mathfrak{H}^{-1}. \tag{S45b}$$

Hankel transform satisfies a similar convolution theorem to the Fourier transform, which follows

$$\mathfrak{H}[A ** B] = 2\pi \mathfrak{H}[A]\mathfrak{H}[B] \tag{S46a}$$
$$\mathfrak{H}^{-1}[A ** B] = 2\pi \mathfrak{H}^{-1}[A]\mathfrak{H}^{-1}[B], \tag{S46b}$$

derived by applying Eq. (S45) to the two-dimensional version of Eq. (S10):

$$\mathfrak{F}_{k_\perp}[A**B] = \frac{1}{C_{\mathfrak{F}}^2}\mathfrak{F}_{k_\perp}[A]\mathfrak{F}_{k_\perp}[B],$$

$$\text{with} A**B = \int_{-\infty}^{\infty}\int_{-\infty}^{\infty} A(x,y)B(X-x,Y-y)dxdy \text{ represents the two-dimensional convolution}$$

$$= \int_0^{2\pi}\int_0^{\infty} A(r)B(|\vec{R}-\vec{r}|)rdrd\theta, \text{ if } A \text{ and } B \text{ are radially symmetric}$$

$$\Rightarrow A**B \text{ is also radially symmetric. (Fig. S10)}$$

With Eq. (S45a), it is transformed into Eq. (S46a). Similar process can be applied to derive Eq. (S46b).

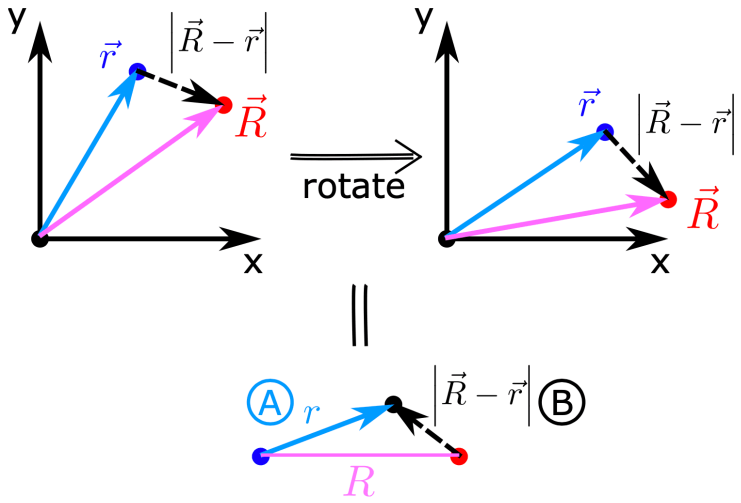

Figure S10. Two-dimensional convolution $A**B$ of two radially-symmetric functions $A(r)$ and $B(r)$. Because A depends only on $\vec{r}$ and B only on $\vec{R}-\vec{r}$, the convolution $(A**B)(R) = \int_0^{2\pi}\int_0^{\infty} A(r)B(\vec{R}-\vec{r})rdrd\theta$ is also radially symmetric. This convolution can be treated as multiplying values depending on the black dot moving over the entire space (bottom figure), whose only independent variable is the distance R between the blue and red dots.

Hankel transform satisfies the Parseval's theorem as well. The two-dimensional Parseval's theorem of the Fourier transform is

$$\frac{1}{C_{\mathfrak{I}\mathfrak{F}}^2}\int_{-\infty}^{\infty}\int_{-\infty}^{\infty}|A(\vec{r}_\perp)|^2dxdy = \frac{1}{C_{\mathfrak{F}}^2}\int_{-\infty}^{\infty}\int_{-\infty}^{\infty}|A(\vec{k}_\perp)|^2dk_xdk_y. \tag{S47}$$

If A is radially symmetric (and thus its 2D Fourier transform $A(\vec{k}_\perp)$ is also radially symmetric [Eq. (S41)]), with Eq. (S45a), it becomes

$$\frac{1}{C_{\mathfrak{I}\mathfrak{F}}^2}2\pi\int_0^{\infty}|A(r_\perp)|^2r_\perp dr_\perp = \frac{1}{C_{\mathfrak{F}}^2}2\pi\int_0^{\infty}\left(|2\pi C_{\mathfrak{F}}^2\right)A_H(k_\perp)|^2k_\perp dk_\perp, \tag{S48}$$

which leads to the Parseval's theorem for the Hankel transform:

$$\int_0^{\infty}|A(r_\perp)|^2r_\perp dr_\perp = \int_0^{\infty}|A_H(k_\perp)|^2k_\perp dk_\perp. \tag{S49}$$

doi.org/10.32388/JFPRSL.2

B. Numerical computation: Fast Hankel transform of high accuracy (FHATHA)

In this section, we will discuss how to numerically compute the Hankel transform with the "fast Hankel transform of high accuracy," which et al.Magni abbreviated as FHATHA[20]. There are a few numerical procedures to compute the Hankel transform, among which one of the most popular is the quasi-fast Hankel transform (QFHT)[21][22]. FHATHA outperforms QFHT by exhibiting two orders of magnitude lower error while relying on the well-established fft that offers computational efficiency.

First, both the fields in real $r_\perp$-space and $k_\perp$-space are sampled at

$$r_{\perp,n} = r_\perp^{\max}\zeta_n \tag{S50a}$$

$$k_{\perp,n} = k_\perp^{\max}\zeta_n, \tag{S50b}$$

where ζ_n represents the normalized coordinate that follows

$$\zeta_n = \zeta_0 e^{\alpha n}, \quad n = 0, 1, \cdots, N_\perp - 1 \tag{S51}$$

with $\zeta_0 = \frac{1+e^\alpha}{2}e^{-\alpha N_\perp}$ such that $\zeta_n, \forall n \geq 1$ are in the center of each interval $[\xi_n, \xi_{n+1}]$. ξ_n is the normalized coordinate following

$$\xi_n = \begin{cases} 0, & n = 0 \\ \xi_0' e^{\alpha n}, & n = 1, 2, \cdots, N_\perp \end{cases}, \tag{S52}$$

where $\xi_0' = e^{-\alpha N_\perp}$ (Fig. S11). α is given such that the widths of the first and the last intervals are the same:

$$\begin{aligned} &\xi_1 - \xi_0 = \xi_{N_\perp} - \xi_{N_\perp - 1} \\ \Rightarrow\ &e^{-\alpha(N_\perp - 1)} = 1 - e^{-\alpha}, \end{aligned} \tag{S53}$$

which can be easily solved numerically. During computing the Hankel transform, the function needs to be evaluated at the center of each interval. However, ζ_0 is not at the center of $[\xi_0, \xi_1]$, as we redefine ξ_0 from ξ_0' to 0 [Eq. (S52)]. Therefore, $A(r_{\perp,0} = r_\perp^{\max}\zeta_0)$ needs to be replaced with $A(r'_{\perp,0} = r_\perp^{\max}\zeta_0')$ (with $\zeta_0' = \xi_1/2$ being at the center of $[\xi_0 = 0, \xi_1]$), which is approximated through extrapolation of $A(r_{\perp,0})$ and $A(r_{\perp,1})$ with a parabola with zero derivative at the origin, a reasonable approximation curve for a radially-symmetric function. In FHATHA, an extra evaluation at $\zeta_{N_\perp}$, beyond the range of Eq. (S51), is required, which is simply treated with $A(r_{\perp,N_\perp} = r_\perp^{\max}\zeta_{N_\perp}) = 0$. If we denote A_n as $A(r_{\perp,n})$, eventually the A that is used in FHATHA is

$$\tilde{A}_n = \begin{cases} A(r'_{\perp,0}) = \ell_0(A_0 - A_1) + A_1, & n = 0 \quad \text{(from the parabola approximation)} \\ A_n, & n = 1, 2, \cdots, N_\perp - 1 \\ 0, & n = N_\perp \end{cases} \tag{S54}$$

where

$$\ell_0 = \frac{e^\alpha(2 + e^\alpha)}{(1 + e^\alpha)^2(1 - e^{-2\alpha})}. \tag{S55}$$

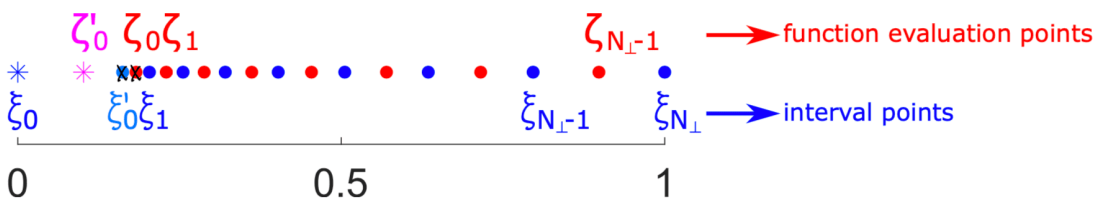

Figure S11. Numerical sampling in FHATHA.

FHATHA solves the Hankel transform by summing over Hankel-transform integral of each interval, whose function is evaluated at ζ_n [Eq. (S51)] (with slight modification at $n = 0$ [Eq. (S54)]) but interval is defined with ξ_n [Eq. (S52)]:

$$\begin{aligned}\int_{r_{\perp,n}}^{r_{\perp,n+1}} A(r_\perp) J_0(k_\perp r_\perp) r_\perp dr_\perp &\approx \tilde{A}_n \int_{r_{\perp,n}}^{r_{\perp,n+1}} J_0(k_\perp r_\perp) r_\perp dr_\perp \\ &= \tilde{A}_n \frac{r_\perp}{k_\perp} J_1(k_\perp r_\perp)\Big|_{r_{\perp,n}}^{r_{\perp,n+1}} \\ &= \frac{\tilde{A}_n}{k_\perp}[r_{\perp,n+1} J_1(k_\perp r_{\perp,n+1}) - r_{\perp,n} J_1(k_\perp r_{\perp,n})] \end{aligned} \tag{S56}$$

by use of the relation $\int J_0(u) u du = u J_1(u) + C$. Summing over all $n = 0, 1, \cdots, (N_\perp - 1)$ leads to

$$\begin{aligned} A_{H,m} = A_H(k_{\perp,m}) &= \frac{1}{k_{\perp,m}} \sum_{n=0}^{N_\perp - 1} \ell_n \left(A_n - A_{n+1}\right) \left(r_\perp^{\max} \xi_{n+1}\right) J_1\left(k_{\perp,m} \left(r_\perp^{\max} \xi_{n+1}\right)\right) \\ &= \frac{r_\perp^{\max}}{k_{\perp,m}} \sum_{n=0}^{N_\perp - 1} \left[\ell_n \left(A_n - A_{n+1}\right) e^{\alpha(n+1-N_\perp)}\right] J_1(k_\perp^{\max} r_\perp^{\max} \zeta_0 e^{\alpha(m+n+1-N_\perp)}) \end{aligned} \tag{S57}$$

where $\ell_n = 1$ if $n \neq 0$, and J_1 is the Bessel function of order 1.

If we define the discrete cross convolution $\star_D$ as

$$(P \star_D Q)_m \equiv \sum_n \overline{P_n} Q_{m+n}. \tag{S58}$$

It satisfies [Eq. (S20a)]

$$\mathfrak{F}_D\left[P \star_D Q\right] = \frac{1}{C_{\mathfrak{F}_D}} \overline{\mathfrak{F}_D[P]} \mathfrak{F}_D[Q] = \frac{1}{C_{\mathfrak{F}_D}} \left(\frac{C_{\mathfrak{F}_D}}{C_{\mathfrak{I}\mathfrak{F}_D}} \mathfrak{F}_D^{-1}[\overline{P}]\right) \mathfrak{F}_D[Q] = \frac{1}{C_{\mathfrak{I}\mathfrak{F}_D}} \mathfrak{F}_D^{-1}[\overline{P}] \mathfrak{F}_D[Q]. \tag{S59}$$

Since DFT inherently exhibits periodicity (Fig. S3), zero-padding is required if P or Q does not display periodicity beyond the sampling window; otherwise, aliasing will occur by direct application of Eq. (S59).

If we let

$$P_n = \overline{R}_n = \begin{cases} \ell_n \left(\overline{A}_n - \overline{A}_{n+1}\right) e^{\alpha(n+1-N_\perp)}, & n = 0, 1, \cdots, N_\perp - 1 \\ 0, & n = N_\perp, N_\perp + 1, \cdots, T^w_{\text{extended}} \quad \text{(zero-padding)} \end{cases} \tag{S60a}$$

$$Q_n = J_1(k_\perp^{\max} r_\perp^{\max} \zeta_0 e^{\alpha(n+1-N_\perp)}), \quad n = 0, 1, \cdots, T^w_{\text{extended}} \tag{S60b}$$

Eq. (S57) becomes

$$A_{H,m} = \frac{r_\perp^{\max}}{k_{\perp,m}} \frac{1}{C_{\mathfrak{I}\mathfrak{F}_D}} \mathfrak{F}_D^{-1}\left[\mathfrak{F}_D^{-1}[R] \mathfrak{F}_D[Q]\right] \tag{S61a}$$

$$\overset{\text{or also}}{=} \frac{r_\perp^{\max}}{k_{\perp,m}} \frac{1}{C_{\mathfrak{F}_D}} \mathfrak{F}_D\left[\mathfrak{F}_D[R] \mathfrak{F}_D^{-1}[Q]\right], \quad \text{derived from Eq. (S20b) with a similar process} \tag{S61b}$$

which is meaningful only for $m = 0, 1, \cdots, (N_\perp - 1)$ with others discarded after FHATHA. The zero-padding range is determined by $T^w_{\text{extended}} \geq 2N_\perp - 2$ [so that there are a total of $(2N_\perp - 1)$ sampling points]. This zero-padding procedure is similar to the convolution operation with clipped extended signals (Fig. S6). However, since the summation in Eq. (S57) includes Q_n up to $n = 2N_\perp - 2$, Q_n must be analytically computed at least for $n = 0, 1, \cdots, (2N_\perp - 2)$, rather than simple zero-padding as in the convolution theorem (Sec. 3). Note that Q can be precomputed only once before the simulation. In the physical Fourier-transform convention ($C_{\mathfrak{F}_\text{D}} = \frac{1}{\mathfrak{N}}$ and thus $C_{\mathfrak{I}\mathfrak{F}_\text{D}} = 1$), $A_{\text{H,m}} = \frac{r_\perp^{\max}}{k_{\perp,m}} \mathfrak{F}_\text{D}^{-1} \left[\mathfrak{F}_\text{D}^{-1}[R]\mathfrak{F}_\text{D}[Q]\right]$, which is (in MATLAB syntax below)

```
A_H = r_max./k.*fft(fft(R).*ifft(Q));
```

Since Hankel transform and inverse Hankel transform exhibit the same form [Eq. (S43)], inverse FHATHA follows Eq. (S61) by swapping the symbols $r \leftrightarrow k$. Note that Q is independent of Hankel or inverse Hankel transforms due to its $(r_\perp, k_\perp)$ symmetry. Fig. S12 shows two verification examples that demonstrate its excellent consistency with the analytical formula.

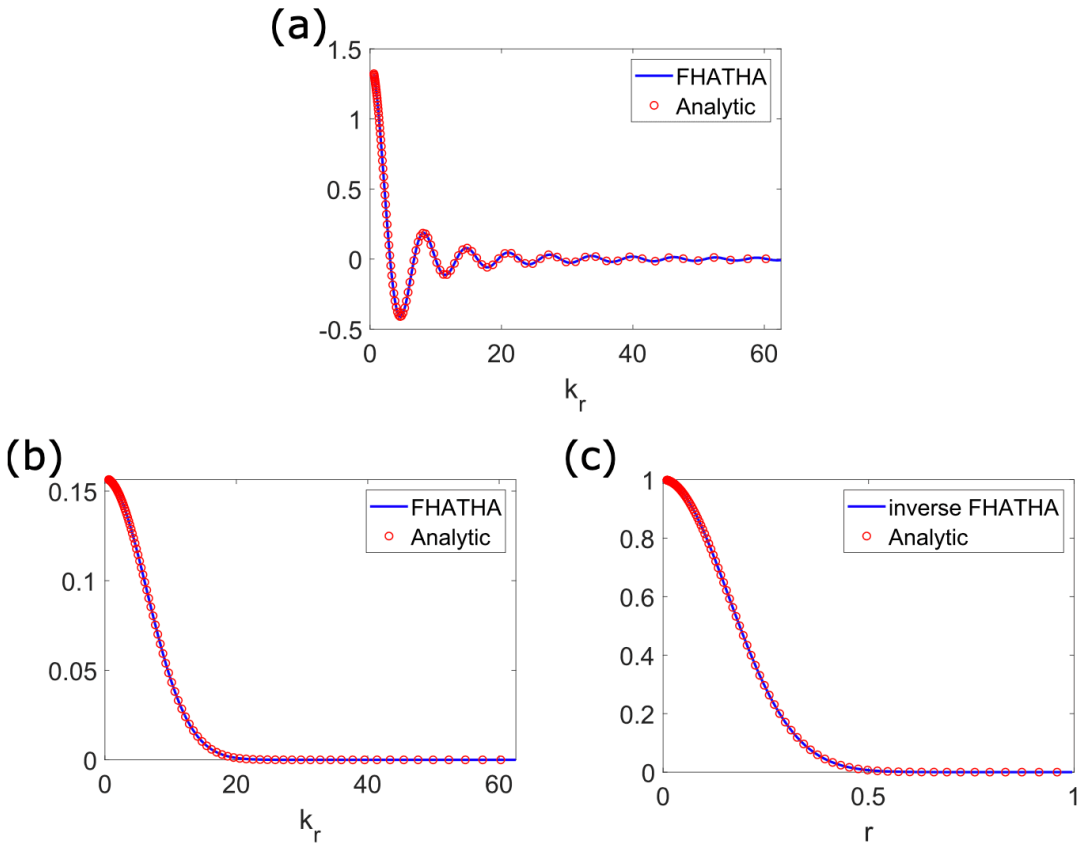

Figure S12. Verifications of FHATHA. Hankel transforms of (a) $f(r) = \sqrt{\frac{5}{2\pi}} r^2$ and (b) $f(r) = e^{-20r^2}$, which are $\sqrt{10\pi} \frac{2\eta J_0(\eta) + (\eta^2 - 4) J_1(\eta)}{\eta^3}$ (with $\eta = r_\perp^{\max} k_\perp$) and $\frac{\pi}{20} e^{-k_\perp^2/80}$, respectively. (c) Inverse Hankel transform of (b). This is used to further verify the operation of inverse Hankel transform and see whether the signal can be recovered.

doi.org/10.32388/JFPRSL.2

The exponential sampling strategy [Eqs. (S51) and (S52)] of FHATHA introduces an advantage over typical uniform sampling. Mostly, the radially-symmetric field is the strongest at the spatial center. In particular, in cases such as self-focusing for a high-peak-power pulse (Fig. S13), the spatial extent of the field decreases as it propagates. This can lead to undersampling of the field, which is resolved by FHATHA's exponential sampling that densely samples around the center.

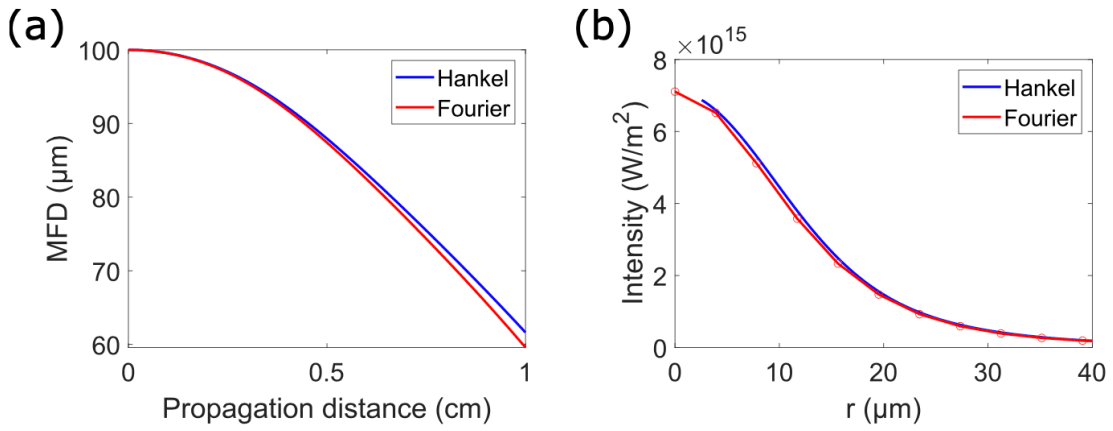

Figure S13. (a) Mode-field-diameter (MFD) evolution of a pulse propagating in a 1-cm long bulk silica, simulated with the Hankel transform or 2D spatial Fourier transform. The input pulse is 1-ps long and has 8-μJ pulse energy, with a Gaussian spatial profile of 100-μm MFD. (b) The intensity profile of the pulse.

Unlike the frequency window in the Fourier transform that is determined by the temporal sampling period, the $k_\perp$ window can be chosen quite arbitrarily. Its value is determined by the signal's maximum $\vec{k}_\perp$ vector.

Footnotes

[1] A rule of thumb for the size of frequency window is that it needs to be around 5--10 times as the pulse bandwidth.

References

1. ^Boyd RW. Nonlinear Optics. 3rd ed. Burlington: Academic Press; 2008. ISBN 978-0-12-369470-6.
2. ^Conforti M, Marini A, Faccio D, Biancalana F (2013). "Negative frequencies get real: a missing puzzle piece in nonlinear opt ics". arXiv preprint arXiv:1305.5264. doi:10.48550/ARXIV.1305.5264. Available from: https://arxiv.org/abs/1305.5264.
3. ^Chen YH, Varma S, York A, Milchberg HM (2007). "Single-shot, space- and time-resolved measurement of rotational wave packet revivals in H_2, D_2, N_2, O_2, and N_2O." Opt. Express. **15** (18): 11341--11357. doi:10.1364/OE.15.011341. Link.
4. a, b Chen YH, Wise F (2024). "Unified and vector theory of Raman scattering in gas-filled hollow-core fiber across temporal r egimes." APL Photonics. 9 (3): 030902. doi:10.1063/5.0189749.
5. ^Konyashchenko AV, Losev LL, Pazyuk VS, Tenyakov SY (2008). "Frequency shifting of sub-100 fs laser pulses by stimulated Raman scattering in a capillary filled with pressurized gas". Appl. Phys. B. 93 (2): 455–461. doi:10.1007/s00340-008-3177-1.

6. ^ Chen YH, Moses J, Wise F (2023). "Femtosecond long-wave-infrared generation in hydrogen-filled hollow-core fiber." J. Opt. Soc. Am. B. **40** (4): 796--806. doi:10.1364/JOSAB.483969. Link to article.
7. ^ Loree TR, Cantrell CD, Barker DL (1976). "Stimulated Raman emission at 9.2 μm from hydrogen gas". Opt. Commun.. **17** (2): 160–162. doi:10.1016/0030-4018(76)90204-2. Link.
8. ^ Grasyuk AZ, Losev LL, Nikogosyan DN, Oraevskii AA (1984). "Generation of single picosecond pulses of up to 0.6 mJ energy and of 9.2 μm wavelength by stimulated Raman scattering." Sov. J. Quantum Electron.. **14** (9): 1257–1258. doi:10.1070/qe1984v014n09abeh006203.
9. ^ Chen YH, Wise F (2024). "A simple accurate way to model noise-seeded ultrafast nonlinear processes." arXiv preprint arXiv: 2410.20567. Available from: https://arxiv.org/abs/2410.20567.
10. ^ Eggleston J, Byer R (1980). "Steady-state stimulated Raman scattering by a multimode laser". IEEE J. Quantum Electron.. **16** (8): 850–853. doi:10.1109/JQE.1980.1070592.
11. ^ Dudley JM, Genty G, Coen S (2006). "Supercontinuum generation in photonic crystal fiber". Rev. Mod. Phys.. **78** (4): 1135–1184. doi:10.1103/RevModPhys.78.1135.
12. ^ Frosz MH (2010). "Validation of input-noise model for simulations of supercontinuum generation and rogue waves." Opt. Express. **18** (14): 14778–14787. doi:10.1364/OE.18.014778. Link to article.
13. ^ Genier E, Bowen P, Sylvestre T, Dudley JM, Moselund P, Bang O (2019). "Amplitude noise and coherence degradation of femtosecond supercontinuum generation in all-normal-dispersion fibers". J. Opt. Soc. Am. B. **36** (2): A161--A167. doi:10.1364/JOSAB.36.00A161. Link to article.
14. ^ Strickland D, Mourou G (1985). "Compression of amplified chirped optical pulses." Optics Communications. **55** (6): 447--449. doi:10.1016/0030-4018(85)90151-8. Link to article.
15. ^ Schulte J, Sartorius T, Weitenberg J, Vernaleken A, Russbueldt P (2016). "Nonlinear pulse compression in a multi-pass cell." Opt. Lett.. **41** (19): 4511–4514. doi:10.1364/OL.41.004511. Link.
16. ^ Hanna M, D\uooe9len X, Lavenu L, Guichard F, Zaouter Y, Druon F, Georges P (2017). "Nonlinear temporal compression in multipass cells: theory." J. Opt. Soc. Am. B. **34** (7): 1340--1347. doi:10.1364/JOSAB.34.001340. Link to article.
17. ^ Centurion M, Porter MA, Pu Y, Kevrekidis PG, Frantzeskakis DJ, Psaltis D (2006). "Modulational Instability in a Layered Kerr Medium: Theory and Experiment". Phys. Rev. Lett.. **97** (23): 234101. doi:10.1103/PhysRevLett.97.234101.
18. ^ Zhang S, Fu Z, Zhu B, Fan G, Chen Y, Wang S, Liu Y, Baltuska A, Jin C, Tian C, Tao Z (2021). "Solitary beam propagation in periodic layered Kerr media enables high-efficiency pulse compression and mode self-cleaning." Light Sci. Appl.. **10**: 53. doi:10.1038/s41377-021-00495-9.
19. ^ Wang W, Eisenberg Y, Chen YH, Xu C, Wise F (2024). "Efficient temporal compression of 10-μJ pulses in periodic layered Kerr media." Opt. Lett.. **49**(20): 5787–5790. doi:10.1364/OL.539381. Link to article.
20. ^ Magni V, Cerullo G, Silvestri SD (1992). "High-accuracy fast Hankel transform for optical beam propagation". J. Opt. Soc. Am. A. **9** (11): 2031–2033. doi:10.1364/JOSAA.9.002031. Link to article.
21. ^ Siegman AE (1977). "Quasi fast Hankel transform". Opt. Lett.. **1** (1): 13–15. doi:10.1364/OL.1.000013. Link to article.
22. ^ Agrawal GP, Lax M (1981). "End correction in the quasi-fast Hankel transform for optical-propagation problems". Opt. Lett.. **6** (4): 171–173. doi:10.1364/OL.6.000171.

Declarations

Funding: No specific funding was received for this work.

Potential competing interests: No potential competing interests to declare.